

Designing Interference-Immune Doppler-Tolerant Waveforms for Radar Applications

Robin Amar, Mohammad Alae-Kerahroodi, Prabhu Babu, and Bhavani Shankar M. R.

Abstract—Dynamic target detection using FMCW waveform is challenging in the presence of interference for different radar applications. Degradation in SNR is irreparable and interference is difficult to mitigate in time and frequency domain. In this paper, a waveform design problem is addressed using the Majorization-Minimization (MM) framework by considering PSL/ISL cost functions, resulting in a code sequence with Doppler-tolerance characteristics of an FMCW waveform and interference immune characteristics of a tailored PMCW waveform (unique phase code + minimal ISL/PSL). The optimal design sequences possess polynomial phase behavior of degree Q amongst its sub-sequences and obtain optimal ISL and PSL solutions with guaranteed convergence. By tuning the optimization parameters such as degree Q of the polynomial phase behavior, sub-sequence length M and the total number of sub-sequences L , the optimized sequences can be as Doppler tolerant as FMCW waveform in one end, and they can possess small cross-correlation values similar to random-phase sequences in PMCW waveform on the other end. If required in the event of acute interference, new codes can be generated in the runtime which have low cross-correlation with the interferers. The performance analysis indicates that the proposed method outperforms the state-of-the-art counterparts.

Index Terms—FMCW, PMCW, Interference, Doppler tolerance, Chirp-like sequences.

I. INTRODUCTION

RADAR has traditionally been associated with military and law enforcement applications due to its development, but it is now a common solution for civil situations. Currently, high-resolution Frequency Modulated Continuous Wave (FMCW) radar sensors operating at 60GHz, 79GHz, and 140GHz with sometimes finer than 10cm range resolution are becoming integral in a variety of applications ranging from automotive safety and autonomous driving [1], [2], indoor positioning [3], [4] to infant and elderly health monitoring [5]. As the penetration of these low-cost high-performance sensors grows, the likelihood of radar signal interference and the associated ghost target problems also grows [6], [7].

The transmit waveform that is commonly used in a large number of modern millimeter wave (mmWave) radar sensors is based on Linear Frequency Modulation (LFM). LFM is well-known in radar literature due to its distinctive properties of large time-bandwidth product (high pulse compression ratio) and high Doppler-tolerance [8], [9]. In automotive FMCW

radars, LFM is typically used as the waveform modulation scheme, since it can be compressed with a very low-cost and efficient technique known-as *de-chirping* operation¹ [10]. The primary benefit of de-chirping is that the received signal can be sampled at much lower rates in comparison to its bandwidth [11]–[13]. Not surprisingly, this advantage has been motivating many manufactures to build their radar system based on FMCW technology. While FMCW remains the most prevalent modulation scheme for mmWave radar sensors, alternate modulation schemes such as Phase Modulated Continuous Wave (PMCW) [14], [15] have been proposed as a way to mitigate interference for different applications [15]–[17]. Using PMCW technology, Doppler-tolerant property can be obtained by using a class of codes characterized by a systematic generation formula [16], such as, Frank [18], P1, P2, P3, and P4 [19], Golomb [20], Chu [21], PAT [22], etc (refer Appendix A for more details). These codes typically exhibit small Peak Sidelobe Level (PSL) and Integrated Sidelobe Level (ISL) values in their aperiodic autocorrelation function; however, they are unfortunately sometimes constrained to the specific lengths [23]. Also, due to a lack of uniqueness in these codes, they are equally vulnerable to mutual interference (MI) similar to FMCW technology. We aim to overcome this limitation in this paper by proposing a framework for designing constant modulus polyphase Doppler-tolerant sequences that are also immune to interference for variety of radar applications.

A. Doppler-Tolerant Waveforms

When a target is stationary, i. e., the Doppler distortions of the returned radar signals can be neglected, then correlation or matched-filter processing is relatively straight-forward [24]. In those applications where high resolution requirements and high target speeds combine, the distortions in the waveform lead to severe degradations, and a knowledge of the Doppler shift of the target should be available, or a bank of mismatched filter needs to be considered in the receive side to compensate loss in Signal to Noise Ratio (SNR) [25]. However, using so-called Doppler-invariant waveforms in the transmit side is a simpler alternative approach to dealing with high Doppler shifts. In this case, even in the presence of an arbitrarily large Doppler shift, the received signal remains matched to the filter, but a range-Doppler coupling may occur as an unintended consequence [24].

It is known that FMCW waveform has the Doppler-tolerant property by its nature. Thus, a possible solution to build PMCW with Doppler-tolerant properties is to mimic the behaviour of FMCW waveforms by using the phase history of a pulse with linearly varying frequency, and building *chirp-like*

¹Also referred to as *stretch processing*.

Robin Amar, SnT, University of Luxembourg, Luxembourg.
email: robin.amar@uni.lu

Mohammad Alae-Kerahroodi and Bhavani Shankar M. R. are with SnT, University of Luxembourg, Luxembourg.

Prabhu Babu is with IIT Delhi.

This work was supported by FNR (Luxembourg) through the CORE project “SPRINGER: Signal Processing for Next Generation Radar” under grant C18/IS/12734677/SPRINGER.

Manuscript received December 16, 2021; revised mm dd, yyyy.

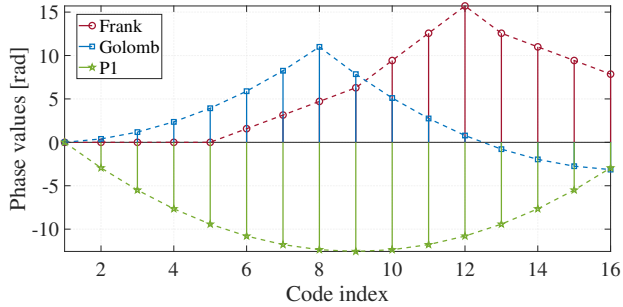


Figure 1: The unwrapped phase values of three polyphase codes of length $N = 16$: Frank, Golomb, and P1.

polyphase sequences [23]. Indeed, because frequency is the derivative of phase, in order to have linear frequency properties like FMCW, the phase variation of PMCW sequences should be quadratic throughout the length of the sequence, as shown in Figure 1 for Frank, Golomb, and P1 sequences of length $N = 16$. Interestingly, chirplike polyphase sequences are known to typically have small PSL and ISL values², the metrics which are strictly connected to the sharpness of the code autocorrelation function [25]–[33].

Recently, several studies have considered the design of polyphase sequences with good Doppler tolerance properties [34]–[41]. In [34] Linear-FM Synthesized (LFM-Syn) waveform has been proposed to achieve low range sidelobes and high Doppler tolerance in the synthesized waveform. The study combines the random noise waveform and the conventional LFM waveform. In [38] a Coordinate Descent (CD)-based approach is proposed for designing waveform with high Doppler tolerance properties. In both [34] and [38], a template-matching objective function is established and optimized to obtain waveforms with low range sidelobes and high Doppler tolerance properties. Unlike the template matching approaches, in [42] a computational approach is proposed for designing polyphase sequences with *piecewise linear phase properties*. Despite the fact designing Frank-like sequences was considered in this paper, the overall quadratic phase trend of this sequence was not taken into account during the proposed optimization framework. As a result, the optimization method mentioned in it does not result in Doppler-tolerant waveforms. Different from designing waveform with Doppler tolerance properties, several studies like [43]–[46] have considered the problem of shaping Ambiguity Function (AF) by minimizing sidelobes on range-Doppler plane around the origin to improve the detection performance. However, the optimized waveform by these studies is not resilient to Doppler shifts.

B. Interference in FMCW Radars

Interference is a well-known and unavoidable problem in many fields. In emerging automotive radar application, the

²PSL shows the maximum autocorrelation sidelobe of a transmit waveform. If this value is not small, then either a false detection or a miss detection may happen. Similar properties hold for ISL of transmitting waveforms where the energy of autocorrelation sidelobes should be small to mitigate the deleterious effects of distributed targets, which are the case for automotive applications.

radar sensors use FMCW as the standard sensing waveform. Vast deployment of FMCW radars in multiple passenger and commercial vehicles has led to a significant vehicle-to-vehicle radar interference. The interference in all these cases is largely due to simultaneous use of shared spectrum when operating in the detection range of the other sensor and the inherent lack of coordination between radars resulting from the lack of a centralized control and resource allocation mechanism [47]–[49].

Further, in this context, FMCW radars experience similar-slope and sweeping slope interference [6], [7] from other sensors operating in the field of view (FoV). Even though sweeping interference can be avoided or repaired (using original signal reconstruction), similar-slope interference is hard to manage [7]. Mitigation techniques are able to address both the interference³ but enhances the average noise resulting in the decrement of SNR [53]. As all the available degrees of freedom (time, operating frequency, bandwidth) to design the FMCW radars has already been exploited, PMCW based sensors are being looked upon as a promising solution to match the sensing performance of FMCW waveform and alleviate the problem of interference.

PMCW radars employ phase codes in their transmitter which are constant modulus and can drive the transmit amplifier at maximum efficiency. These waveforms are highly immune to interference as every radar may employ its own unique phase code with small auto- and cross-correlation sidelobes [15], [54]. On the flip side, it suffers from Doppler intolerance which makes it hard to employ in high-speed applications. In the case study of the automotive scenarios, the high speed of the targets may result in SNR reduction if the transmit waveform is not Doppler tolerant.

C. Contribution

The idea of this framework is to design polyphase sequences that have good Doppler-tolerance properties and sharp autocorrelation functions. Unlike FMCW, potentially distinct PMCW sequences meeting these requirements exist. This richness in selection of PMCW sequences allows for better interference management than FMCW. In this context, we propose a methodology for generating such a rich set of sequences which can be integrated into existing optimization-based waveform design tools (like Cyclic Algorithm New (CAN) [26], monotonic minimizer for integrated sidelobe level (MISL) [55], Monotonic Minimizer for the ℓ_p -norm of autocorrelation sidelobes (MM-PSL) [27], etc.) to provide the designed waveforms with Doppler tolerance properties.

The main contributions of this work can be summarized as follows:

- *Optimization framework*: The problem formulation leads to an objective function which considers the design of phase sequences with polynomial behavior while simultaneously considering other important properties like ISL

³Although a comprehensive solution to mutual interference still remains an open issue, there has been some prior work in the design of mitigation techniques to diminish the problem of interference [50]–[52].

and PSL. Although ISL and PSL minimization has considered earlier, but all these properties are not addressed simultaneously in literature.

- *Doppler tolerance*: The optimization problem can handle phase sequences with a degree Q polynomial behavior while building on the literature of ℓ_p norm minimization for generic objective subsuming ISL and PSL. Using Majorization-Minimization (MM) based approach, we design sequences with superior properties as compared to the conventional sequences mentioned in literature. Doppler tolerance property arises in a sequence when its phase changes in a quadratic manner (i.e. $Q = 2$). As this is being handled directly in the objective function, the resultant sequence is bound to have better performance for moving targets.
- *Flexibility of design - divide and conquer interference*: This approach offers the flexibility of having multiple sub-sequences, designed in parallel while optimizing the ISL and PSL of the entire sequence. Since each sub-sequence has unique polynomial phase coefficients of degree Q , length, and code, the entire sequence can avoid interference. This provides an additional degree of freedom for waveform design by partitioning the entire sequence into multiple sub-sequences of varying lengths which enables us to tune the optimization variable and generate diverse waveforms whose AF is varying from *Thumbtack type* on one extreme to *Doppler-Tolerant type* on the other end. The proposed formulation provides the possibility of designing sequences of any length N with piecewise polynomial phase behavior amongst its L sub-sequences each of length M_l where $N = M_1 + M_2 + \dots + M_L$ if the sub-sequences have different lengths. This approach can be considered for the scenarios in which sequence lengths other than perfect square (unlike Frank) are required.
- *Application in automotive scenarios*: A simulation environment is created which generates various automotive scenarios where interference is possible. Using the proposed optimization framework, different sequences have been generated and utilized to interfere with each other. The results of the simulation indicate high interference immunity in sensing. This alleviates the necessity for the requirement of additional sensing and communication protocol for safe operation in dense automotive scenarios where MI is possible amongst multiple cars equipped with radar sensors.

Finally, by using the proposed method, one can construct many new such polyphase sequences which were not known and/or could not be constructed by the previous formulations in the literature. Thus, the proposed approach is capable of generating unique sequences which in turn would lead to decrement in the interference amongst multiple sensors operating in the nearby region.

D. Organization and Notations

The rest of this paper is organized as follows. In Section II, we formulate the ℓ_p -norm minimization for designing polynomial phase sequences under unimodular and polynomial phase

constraints. In Section III, we develop an algorithm based on MM framework, where we use a majorizing function to find the optimal solution of the design problem. In Section IV we provide numerical experiments to verify the effectiveness of proposed algorithm. Finally, Section V concludes the paper.

Notation: Boldface upper case letters denote matrices, boldface lower case letters denote column vectors, and italics denote scalars. \mathbb{Z} , \mathbb{R} and \mathbb{C} denote the integer, real and complex field, respectively. $\Re(\cdot)$ and $\Im(\cdot)$ denote the real and imaginary part respectively. $\arg(\cdot)$ denotes the phase of a complex number. The superscripts $(\cdot)^T$, $(\cdot)^*$, $(\cdot)^H$ and $(\cdot)^\dagger$ denote transpose, complex conjugate, conjugate transpose, and pseudo-inverse respectively. $X_{i,j}$ denotes the $(i,j)^{th}$ element of a matrix and x_i denotes the i^{th} element of vector \mathbf{x} . $\text{Diag}(\mathbf{X})$ is a column vector consisting of all the diagonal elements of \mathbf{X} . $\text{Diag}(\mathbf{x})$ is a diagonal matrix formed with \mathbf{x} as its principal diagonal. $\text{vec}(\mathbf{X})$ is a column vector consisting of all the columns of \mathbf{X} stacked.

II. PROBLEM FORMULATION

Let $\{x_n\}_{n=1}^N$ be the transmitted complex unit-modulus radar code sequence of length N . The aperiodic autocorrelation of the transmitting waveform at lag k (e.g. matched filter output at the PMCW radar receiver) is defined as

$$r_k = \sum_{n=1}^{N-k} x_n x_{n+k}^* = r_{-k}^*, \quad k \in [0, \dots, N-1]. \quad (1)$$

The ISL and PSL can be mathematically defined by

$$\text{ISL} = \sum_{k=1}^{N-1} |r_k|^2, \quad (2)$$

$$\text{PSL} = \max_{k=1,2,\dots,N-1} |r_k|. \quad (3)$$

It is clear that the ISL metric is the squared ℓ_2 -norm of the autocorrelation sidelobes. Further, the ℓ_∞ -norm of autocorrelation sidelobes of a sequence is the PSL metric. These can, in fact, be generalized by considering the ℓ_p norm, $p \geq 1$ which offers additional flexibility in design while subsuming ISL and PSL. In general ℓ_p -norm metric of the autocorrelation sidelobes is defined as

$$\left(\sum_{k=1}^{N-1} |r_k|^p \right)^{1/p}, \quad 2 \leq p < \infty. \quad (4)$$

Sequences are designed to minimize the various ℓ_p norm metric in literature [27], [29], [55]–[57]. It is known that in general longer the code, better are the ISL/PSL [27], but the system suffers from high design complexity. One possible solution for reducing complexity is to design long sequences with multiple segments, which is considered in this paper. Let the sequence $\{x_n\}_{n=1}^N$ be partitioned into L sub-sequences each having length of M_l , where $l \in \{1, 2, \dots, L\}$ such that every sub-sequence of it, say

$$\tilde{\mathbf{x}}_l = [x_{\{1,l\}}, x_{\{2,l\}}, \dots, x_{\{M_l,l\}}]^T \in \mathbb{C}^{M_l}, \quad (5)$$

has a polynomial phase, which can be expressed as

$$\arg(x_{\{m,l\}}) = \sum_{q=0}^Q a_{\{q,l\}} m^q, \quad (6)$$

where $a_{\{q,l\}}$ is the Q^{th} degree polynomial coefficient for the phase of the l -th sub-sequence with $q \in \{0, 1, 2, \dots, Q\}$, and $l = 1, \dots, L$. Further,

$$\tilde{\mathbf{X}} = [\tilde{\mathbf{x}}_1, \tilde{\mathbf{x}}_2, \dots, \tilde{\mathbf{x}}_L] \in \mathbb{C}^N, \quad (7)$$

is a collection of all the sub-sequences where $\{x_n\}_{n=1}^N = \text{vec}(\tilde{\mathbf{X}})$. It can be observed that the length of each sub-sequence can be arbitrarily chosen. The problem of interest is to design the code vector $\{x_n\}_{n=1}^N$ with a generic polynomial phase of a degree Q in its sub sequences while having impulse-like autocorrelation function. Therefore, by considering $\sum_{k=1}^{N-1} |r_k|^p$ as the objective function, the optimization problem can be compactly written as

$$\mathcal{P}_1 \begin{cases} \text{minimize} & \sum_{k=1}^{N-1} |r_k|^p \\ \text{subject to} & \arg(x_{\{m,l\}}) = \sum_{q=0}^Q a_{\{q,l\}} m^q, \\ & |x_{\{m,l\}}| = 1, \end{cases} \quad (8)$$

where $m = 1, \dots, M_l$, and $l = 1, \dots, L$.

In the following section, we propose an efficient algorithm to design a set of sub-sequences with polynomial phase relationship of degree Q amongst its sub-sequences based on MM framework.

The MM (majorization-minimization) - is an approach to solve optimization problems that are difficult to solve directly. The principle behind the MM method is to transform a difficult problem into a series of simple problems. Suppose, we want to minimize $f(\mathbf{x})$ over $\mathcal{X} \subseteq \mathbb{C}$. Instead of minimizing the cost function $f(\mathbf{x})$ directly, the MM approach optimizes the sequence of approximate objective functions that majorize $f(\mathbf{x})$. More specifically, starting from a feasible point $\mathbf{x}^{(0)}$, the algorithm produces a sequence $\mathbf{x}^{(i)}$ according to the following update rule

$$\mathbf{x}^{(i+1)} \in \arg \min_{\mathbf{x} \in \mathcal{X}} u(\mathbf{x}, \mathbf{x}^{(i)}), \quad (9)$$

where $\mathbf{x}^{(i)}$ is the point generated by the algorithm at iteration i , and $u(\mathbf{x}, \mathbf{x}^{(i)})$ is the majorization function of $f(\mathbf{x})$ at $\mathbf{x}^{(i)}$. Formally, the function $u(\mathbf{x}, \mathbf{x}^{(i)})$ is said to majorize the function $f(\mathbf{x})$ at the point $\mathbf{x}^{(i)}$ if

$$\begin{aligned} u(\mathbf{x}, \mathbf{x}^{(i)}) &\geq f(\mathbf{x}), \forall \mathbf{x} \in \mathcal{X}, \\ u(\mathbf{x}^{(i)}, \mathbf{x}^{(i)}) &= f(\mathbf{x}^{(i)}), \\ \nabla u(\mathbf{x}^{(i)}, \mathbf{x}^{(i)}) &= \nabla f(\mathbf{x}^{(i)}). \end{aligned} \quad (10)$$

In other words, function $u(\mathbf{x}, \mathbf{x}^{(i)})$ is an upper bound of $f(\mathbf{x})$ over \mathcal{X} and coincides with $f(\mathbf{x})$ at $\mathbf{x}^{(i)}$. To summarize, in order to minimize $f(\mathbf{x})$ over $\mathcal{X} \subseteq \mathbb{C}^n$, the main steps of the majorization-minimization scheme are:

- 1) Find a feasible point $\mathbf{x}^{(0)}$ and set $i = 0$.

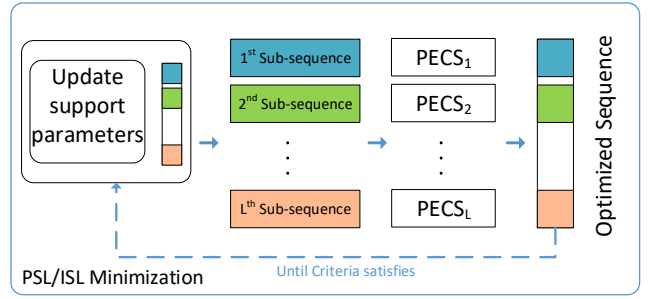


Figure 2: Workflow of PECS for PSL/ISL Minimization.

- 2) Construct a function $u(\mathbf{x}, \mathbf{x}^{(i)})$ that majorizes $f(\mathbf{x})$ at $\mathbf{x}^{(i)}$ and is easier to optimize.
- 3) Let $\mathbf{x}^{(i+1)} \in \arg \min_{\mathbf{x} \in \mathcal{X}} u(\mathbf{x}, \mathbf{x}^{(i)})$.
- 4) If some convergence criterion is met, exit; otherwise, set $i = i + 1$ and go to step (2).

It is easy to show that with this scheme, the objective value is monotonically decreasing at every iteration, i.e.,

$$f(\mathbf{x}^{(i+1)}) \leq u(\mathbf{x}^{(i+1)}, \mathbf{x}^{(i)}) \leq u(\mathbf{x}^{(i)}, \mathbf{x}^{(i)}) = f(\mathbf{x}^{(i)}). \quad (11)$$

The first inequality and the third equality follow from the properties of the majorization function, namely (10) and the second inequality follows from (9). The monotonicity makes MM algorithms very stable in practice. For more details on MM framework, refer [56], [58], [59] and references therein.

III. PROPOSED METHOD

The optimization problem mentioned in (8) is hard to solve since each \mathbf{r}_k is quadratically related to $\{x_n\}_{n=1}^N$ and each $\{x_n\}_{n=1}^N$ is non-linearly related to $a_{\{q,l\}}$. Moreover, the ℓ_p norm of autocorrelation sidelobes becomes difficult to solve using classical optimization approach. As a result MM is considered and after several majorization steps (refer Appendix-B), simplifies to the following optimization problem

$$\mathcal{P}_2 \begin{cases} \text{minimize} & \|\mathbf{x} - \mathbf{y}\|_2 \\ \text{subject to} & \arg(x_{\{m,l\}}) = \sum_{q=0}^Q a_{\{q,l\}} m^q, \\ & |x_{\{m,l\}}| = 1, \end{cases} \quad (12)$$

where

$$\mathbf{y} = (\lambda_{\max}(\mathbf{L})N + \lambda_u) \mathbf{x}^{(i)} - \tilde{\mathbf{R}}\mathbf{x}^{(i)},$$

with λ_{\max} , \mathbf{L} , N , λ_u and $\tilde{\mathbf{R}}$ defined in Appendix B. Note that in [27] the polynomial phase constraint was not considered. Since the objective in (12) is separable in the sequence variables, the minimization problem can now be split into L sub-problems (each of which can be solved in parallel). Let us define, $\rho = |\mathbf{y}|$, and $\psi = \arg(\mathbf{y})$, where ρ_m and ψ_m are the magnitude and phase of every entry of \mathbf{y} , respectively. Also, for ease of notation let us assume that the polynomial phase coefficients and sub-sequence length of the l -th sub-sequence, say $a_{\{q,l\}}$ and M_l are indicated as \tilde{a}_q and \tilde{M} respectively. Thus, dropping

the subscript- l , each of the sub-problem can be further defined as

$$\mathcal{P}_3 \left\{ \underset{\tilde{a}_q}{\text{minimize}} \sum_{m=1}^{\tilde{M}} \left| e^{j(\sum_{q=0}^Q \tilde{a}_q m^q)} - \rho_m e^{j\psi_m} \right|^2, \quad (13) \right.$$

where we have considered the unimodular and polynomial phase constraints of Problem \mathcal{P}_2 directly in the definition of the code entries in Problem \mathcal{P}_3 . Further, the above problem can be simplified as

$$\left\{ \underset{\tilde{a}_q}{\text{minimize}} - \left[\sum_{m=1}^{\tilde{M}} \rho_m \cos \left(\sum_{q=0}^Q \tilde{a}_q m^q - \psi_m \right) \right]. \quad (14) \right.$$

The ideal step would be to minimize the majorized function in (14) for \tilde{a}_q given the previous value of $\tilde{a}_q^{(i)}$, the objective function can be upper-bounded (at a given $\tilde{a}_q^{(i)}$). However, since the optimization variables are in the argument of the cosine function in the objective of 14, the solution to this problem is not straight-forward. Hence, we resort to a second MM step. Towards this, let us define⁴

$$\theta_m = \sum_{q=0}^Q \tilde{a}_q m^q - \psi_m,$$

a majorizer ($g(\theta_m, \theta_m^{(i)})$) of the function $f(\theta_m) = -\rho_m \cos(\theta_m)$ can be obtained by

$$\begin{aligned} g(\theta_m, \theta_m^{(i)}) &= -\rho_m \cos(\theta_m^{(i)}) + (\theta_m - \theta_m^{(i)}) \rho_m \sin(\theta_m^{(i)}) + \\ &\frac{1}{2} (\theta_m - \theta_m^{(i)})^2 \rho_m \cos(\theta_m^{(i)}) \geq -\rho_m \cos(\theta_m), \end{aligned} \quad (15)$$

where θ_m is the variable and $\theta_m^{(i)}$ is the phase value of the last iteration. This follows from exploiting the fact that if a function is continuously differentiable with a Lipschitz continuous gradient, then second order Taylor expansion can be used as a majorizer [56]. Using the aforementioned majorizer function, at i -th iteration of MM algorithm, the optimization problem

$$\mathcal{P}_4 \left\{ \underset{\tilde{a}_q}{\text{minimize}} \sum_{m=1}^{\tilde{M}} \left[-\rho_m \cos(\theta_m^{(i)}) + (\theta_m - \theta_m^{(i)}) \rho_m \sin(\theta_m^{(i)}) + \frac{1}{2} (\theta_m - \theta_m^{(i)})^2 \rho_m \cos(\theta_m^{(i)}) \right] \quad (16) \right.$$

The objective function in (16) can be rewritten into perfect square form and the constant terms independent to the optimization variable \tilde{a}_q can be ignored. Thus, a surrogate optimization problem deduced from (16) is given below

$$\mathcal{P}_5 \left\{ \underset{\tilde{a}_q}{\text{minimize}} \sum_{m=1}^{\tilde{M}} \left[-\rho_m \cos(\theta_m^{(i)}) \left(\sum_{q=0}^Q \tilde{a}_q m^q \right) + \tilde{b}_m \right]^2 \quad (17) \right.$$

where $\tilde{b}_m = -\rho_m \cos(\theta_m^{(i)}) (\psi_m + \theta_m^{(i)}) + \rho_m \sin(\theta_m^{(i)})$.

Now, considering a generic sub-sequence index l we define

$$\boldsymbol{\eta} = [1, 2, 3, \dots, \tilde{M}]^T \in \mathbb{Z}^{\tilde{M}},$$

⁴ θ_m depends on the optimization variables \tilde{a}_q .

Table I: Supporting parameters for Algorithm 1

S.No	Parameter	Relation
1	\mathbf{F}	$2N \times 2N$ FFT Matrix with $F_{m,n} = e^{-j \frac{2mn\pi}{2N}}$
2	f	$\mathbf{F}[\mathbf{x}^{(i)T}, \mathbf{0}_{1 \times N}]$
3	\mathbf{r}	$\frac{1}{2N} \mathbf{F}^H \mathbf{f} ^2$
4	t	$\ \mathbf{r}_{2:N}\ _p$
5	a_k	$\frac{1+(p-1) \left(\frac{ r_{k+1} }{t} \right)^p - p \left(\frac{ r_{k+1} }{t} \right)^{p-1}}{(t - r_{k+1})^2}$
6	\hat{w}_k	$\frac{p}{2t^2} \left(\frac{ r_{k+1} }{t} \right)^{p-2}, k = 1, \dots, N-1$
7	$\tilde{\mathbf{c}}$	$\mathbf{r} \circ [\hat{w}_1, \dots, \hat{w}_{N-1}, 0, \hat{w}_{N-1}, \dots, \hat{w}_1]^T$
8	$\tilde{\boldsymbol{\mu}}$	$\mathbf{F}\tilde{\mathbf{c}}$
9	λ_L	$\max_k \{\tilde{\alpha}_k(N-k) k = 1, \dots, N\}$
10	λ_u	$\frac{1}{2} (\max_{(1 \leq i \leq N)} \tilde{\mu}_{2i} + \max_{(1 \leq i \leq N)} \tilde{\mu}_{2i-1})$

Algorithm 1 PECS

Require: Seed sequence $\mathbf{x}^{(0)}$, N , \tilde{M} , L and p

Ensure: \mathbf{x}

- 1: Set $i = 0$, initialize $\mathbf{x}^{(0)}$.
 - 2: **while** stopping criterion is not met **do**
 - 3: Calculate $\mathbf{F}, \tilde{\boldsymbol{\mu}}, \mathbf{f}, \lambda_L, \lambda_u$ from Table I
 - 4: $\mathbf{y} = \mathbf{x}^{(i)} - \frac{\mathbf{F}_{:,1:N}(\tilde{\boldsymbol{\mu}} \circ \mathbf{f})}{2N(\lambda_L N + \lambda_u)}$
 - 5: $\boldsymbol{\psi} = \arg(\mathbf{y}) \mid \boldsymbol{\psi} = [\tilde{\psi}_1, \dots, \tilde{\psi}_L]^T, \tilde{\psi}_l \in \mathbb{R}^{\tilde{M}}$
 - 6: $\boldsymbol{\rho} = |\mathbf{y}| \mid \boldsymbol{\rho} = [\tilde{\rho}_1, \dots, \tilde{\rho}_L]^T, \tilde{\rho}_l \in \mathbb{R}^{\tilde{M}}$
 - 7: **for** $l \leftarrow 1$ to L **do**
 - 8: $\tilde{\boldsymbol{\psi}}_l = [\psi_1, \dots, \psi_{\tilde{M}}]^T$
 - 9: $\tilde{\boldsymbol{\rho}}_l = [\rho_1, \dots, \rho_{\tilde{M}}]^T$
 - 10: $\theta_m^{(i)} = \sum_{q=0}^Q \tilde{a}_q m^q - \psi_m, m = 1, \dots, \tilde{M}$
 - 11: $\tilde{b}_m = -\rho_m \cos(\theta_m^{(i)}) (\psi_m + \theta_m^{(i)}) + \rho_m \sin(\theta_m^{(i)})$
 - 12: $\boldsymbol{\eta} = [1, 2, 3, \dots, \tilde{M}]^T \in \mathbb{Z}^{\tilde{M}}$
 - 13: $\tilde{\mathbf{A}} = [\eta^0, \eta^1, \dots, \eta^Q] \in \mathbb{Z}^{\tilde{M} \times Q}$,
 - 14: $\mathbf{z} = [\tilde{a}_0, \tilde{a}_1, \dots, \tilde{a}_Q]^T \in \mathbb{R}^Q$
 - 15: $\tilde{\mathbf{b}} = [\tilde{b}_1, \tilde{b}_2, \dots, \tilde{b}_{\tilde{M}}]^T \in \mathbb{R}^{\tilde{M}}$
 - 16: $\mathbf{z}^* = \tilde{\mathbf{A}}^{(t)} \tilde{\mathbf{b}}$
 - 17: $\tilde{\mathbf{x}}_l = e^{j(\tilde{\mathbf{A}}\mathbf{z}^*)}$
 - 18: $\tilde{\mathbf{X}} = [\tilde{\mathbf{x}}_1, \tilde{\mathbf{x}}_2, \dots, \tilde{\mathbf{x}}_L]$
 - 19: $\mathbf{x}^{(i+1)} = \text{vec}(\tilde{\mathbf{X}})$
 - 20: $i \leftarrow i + 1$
- return** $\mathbf{x}^{(i+1)}$

$\boldsymbol{\eta}^q$ implying each element of $\boldsymbol{\eta}$ is raised to the power of q , $q = 0, 1, \dots, Q$. Further,

$$\begin{aligned} \boldsymbol{\gamma} &= \rho_m \cos(\theta_m^{(i)}) \odot [1, \dots, 1]^T \in \mathbb{R}^{\tilde{M}}, \\ \tilde{\mathbf{A}} &= \text{Diag}(\boldsymbol{\gamma})[\boldsymbol{\eta}^0, \boldsymbol{\eta}^1, \dots, \boldsymbol{\eta}^Q] \in \mathbb{Z}^{\tilde{M} \times Q}, \\ \mathbf{z} &= [\tilde{a}_0, \tilde{a}_1, \dots, \tilde{a}_Q]^T \in \mathbb{R}^Q, \\ \tilde{\mathbf{b}} &= [\tilde{b}_1, \tilde{b}_2, \dots, \tilde{b}_{\tilde{M}}]^T \in \mathbb{R}^{\tilde{M}}, \end{aligned} \quad (18)$$

the optimization problem in (17) can be rewritten as

$$\left\{ \underset{\mathbf{z}}{\text{minimize}} \quad \|\tilde{\mathbf{A}}\mathbf{z} - \tilde{\mathbf{b}}\|_2^2, \quad (19) \right.$$

which is the standard Least Squares (LS) problem. As a result, the optimal $\mathbf{z}^* = \tilde{\mathbf{A}}^{(t)} \tilde{\mathbf{b}} = [\tilde{a}_0^*, \tilde{a}_1^*, \dots, \tilde{a}_Q^*]^T$ would

be calculated⁵ and the optimal sequence will be synthesized.

Using the aforementioned setup for a generic sub-sequence index l , we calculate all the $\tilde{\mathbf{x}}_l$ s pertaining to different sub-sequences and derive $\tilde{\mathbf{X}}$. The sequence for the next iteration is derived by vectorizing $\tilde{\mathbf{X}}$ where vector length is again N . The algorithm successively improves the objective and an optimal value of \mathbf{x} is achieved. Details of the implementation for the proposed method in the form of pseudo code are summarized in Algorithm 1⁶ and would be referred further as Polynomial phase Estimate of Coefficients for unimodular Sequences (PECS).

Remark 1: Computational complexity

Assuming L sub-sequences are processed in parallel, the computational load of Algorithm - 1 is dependent on deriving (i) the supporting parameters: \mathbf{f} , \mathbf{r} , t , \mathbf{a} and $\hat{\mathbf{w}}$ mentioned in Table I and (ii) the least squares operation in every iteration of the algorithm. In (i), the order of computational complexity is $\mathcal{O}(2N)$ real additions/subtractions, $\mathcal{O}(Np)$ real multiplications, $\mathcal{O}(N)$ real divisions and $\mathcal{O}(N \log_2 N)$ for Fast Fourier Transform (FFT). In (ii), assume $M_1 = M_2 = \dots = M_l = M$ for simplicity, therefore, the complexity of least squares operation: $\mathcal{O}(M^2Q) + \mathcal{O}(Q^2M) + \mathcal{O}(QM)$ real matrix multiplications and $\mathcal{O}(Q^3)$ real matrix inversion [60] [61]. Therefore, the overall computational complexity is $\mathcal{O}(M^2Q)$ (provided $M > Q$ which is true in general). In case the L sub-sequences are processed sequentially, the complexity is $\mathcal{O}(M^2LQ)$.

Extension of other methods to PECS

In the previous section, by applying a constraint of Q -th degree polynomial phase variation on the sub-sequences, we have addressed the problem of minimizing the autocorrelation sidelobes to obtain optimal ISL/PSL of the complete sequence using ℓ_p norm minimization with the method MM-PSL.

1) *Extension of MISL*: In [26], the ISL metric minimization is addressed with a different approach. As discussed previously in (2), it is just the squared ℓ_2 -norm of the autocorrelation sidelobes. Therefore, the ISL minimization problem under piece-wise polynomial phase constraint of degree Q can be written as follows

$$\mathcal{M}_1 \begin{cases} \text{minimize}_{a_{\{q,l\}}} & \sum_{k=1}^{N-1} |r_k|^2 \\ \text{subject to} & \arg(x_{\{m,l\}}) = \sum_{q=0}^Q a_{\{q,l\}} m^q, \\ & |x_{\{m,l\}}| = 1, \quad m = 1, \dots, M, \\ & l = 1, \dots, L. \end{cases} \quad (20)$$

where $a_{\{q,l\}}$ indicate the coefficients of l -th segment of the optimized sequence whose phase varies in accordance to the degree of the polynomial Q . It has been shown in [26]

⁵We can use "lsqr" in *Sparse Matrices Toolbox* of MATLAB 2021a to solve (19).

⁶MATLAB codes of Algorithm 1 can be shared per request.

that the ISL metric of the aperiodic autocorrelations can be equivalently expressed in the frequency domain as

$$\text{ISL} = \frac{1}{4N} \sum_{g=1}^{2N} \left[\left| \sum_{n=1}^N x_n e^{-j\omega_g(n-1)} \right|^2 - N \right]^2 \quad (21)$$

where $\omega_g = \frac{2\pi}{2N}(g-1)$, $g = 1, \dots, 2N$. Let us define $\mathbf{x} = [x_1, x_2, \dots, x_N]^T$, $\mathbf{b}_g = [1, e^{j\omega_g}, \dots, e^{j\omega_g(N-1)}]^T$, where $g = 1, \dots, 2N$. Therefore, writing (21) in a compact form

$$\text{ISL} = \sum_{g=1}^{2N} (\mathbf{b}_g^H \mathbf{x} \mathbf{x}^H \mathbf{b}_g)^2 \quad (22)$$

The ISL in (22) is quartic with respect to \mathbf{x} and its minimization is still difficult. The MM based algorithm (MISL) developed in [55] computes a minimizer of (22). So given any sequence \mathbf{x} , the surrogate minimization problem in MISL algorithm is given by

$$\mathcal{M}_2 \begin{cases} \text{minimize}_{a_{\{q,l\}}} & \Re(\mathbf{x}^H (\hat{\mathbf{A}} - 2N^2 \mathbf{x}^{(i)} (\mathbf{x}^{(i)H})) \mathbf{x}^{(i)}) \\ \text{subject to} & \arg(x_{\{m,l\}}) = \sum_{q=0}^Q a_{\{q,l\}} m^q \\ & |x_{\{m,l\}}| = 1. \end{cases} \quad (23)$$

where $\mathbf{A} = [b_1, \dots, b_{2N}]$, $\mathbf{f}^{(i)} = |\mathbf{A}^H \mathbf{x}^{(i)}|^2$, $f_{\max}^{(i)} = \max_f \{f_g^{(i)} : g = 1, \dots, 2N\}$, $\hat{\mathbf{A}} = \mathbf{A}(\text{Diag}(\mathbf{f}^{(i)}) - f_{\max}^{(i)} \mathbf{I}) \mathbf{A}^H$. The problem in (23) is majorized once again and the surrogate minimization problem is given as

$$\mathcal{M}_3 \begin{cases} \text{minimize}_{a_{\{q,l\}}} & \|\mathbf{x} - \mathbf{y}\|_2 \\ \text{subject to} & \arg(x_{\{m,l\}}) = \sum_{q=0}^Q a_{\{q,l\}} m^q \\ & |x_{\{m,l\}}| = 1. \end{cases} \quad (24)$$

where $\mathbf{y} = -\mathbf{A}(\text{Diag}(\mathbf{f}^{(i)}) - f_{\max}^{(i)} \mathbf{I}) \mathbf{A}^H \mathbf{x}^{(i)}$. Once the optimization problem in (24) is achieved, i.e \mathcal{M}_3 , it is exactly equal to the problem in (12), i.e. \mathcal{P}_2 and hence its solution can be pursued further. The details of the implementation can be found in Algorithm 2 and 3.

2) *Extension of CAN*: In addition to the above mentioned procedure using MM-PSL, the optimization problem in (20) can also be solved using CAN method [26]. As opposed to the approach pursued in [55] of directly minimizing a quartic function, in [26] the solution of the objective function in (20) is assumed to be "almost equivalent" to minimizing a quadratic function

$$\text{minimize}_{\{x_n\}_{n=1}^N; \{\psi_g\}_{g=1}^{2N}} \sum_{g=1}^{2N} \left| \sum_{n=1}^N x_n e^{-j\omega_g n} - \sqrt{N} e^{j\psi_g} \right|^2 \quad (25)$$

It can be written in a more compact form (to within a multiplicative constant)

$$\|\mathbf{A}^* \bar{\mathbf{x}} - \mathbf{v}\|^2 \quad (26)$$

Algorithm 2 PECS subroutine

```

1: procedure PECS( $\mathbf{y}^{(i)}, L, M_l, a_{q,l}^{(i)}$ )
2:    $\boldsymbol{\psi} = \arg(\mathbf{y}) \mid \boldsymbol{\psi} = [\tilde{\boldsymbol{\psi}}_1^T, \dots, \tilde{\boldsymbol{\psi}}_L^T]^T, \tilde{\boldsymbol{\psi}}_l \in \mathbb{R}^{M_l}$ 
3:    $\boldsymbol{\rho} = |\mathbf{y}| \mid \boldsymbol{\rho} = [\tilde{\boldsymbol{\rho}}_1^T, \dots, \tilde{\boldsymbol{\rho}}_L^T]^T, \tilde{\boldsymbol{\rho}}_l \in \mathbb{R}^{M_l}$ 
4:   for  $l \leftarrow 1$  to  $L$  do
5:      $\tilde{\boldsymbol{\psi}}_l = [\psi_1, \dots, \psi_{M_l}]^T$ 
6:      $\tilde{\boldsymbol{\rho}}_l = [\rho_1, \dots, \rho_{M_l}]^T$ 
7:      $\theta_m^{(i)} = \sum_{q=0}^Q \tilde{a}_q m^q - \psi_m, m = 1, \dots, M_l$ 
8:      $\tilde{b}_m = -\rho_m \cos \theta_m^{(i)} (\psi_m + \theta_m^{(i)}) + \rho_m \sin \theta_m^{(i)}$ 
9:      $\boldsymbol{\eta}_l = [1, 2, 3, \dots, M_l]^T \in \mathbb{Z}^{M_l}$ 
10:     $\mathbf{A} = [\boldsymbol{\eta}^0, \boldsymbol{\eta}^1, \dots, \boldsymbol{\eta}^Q] \in \mathbb{Z}^{M_l \times Q}$ 
11:     $\mathbf{z} = [\tilde{a}_0, \tilde{a}_1, \dots, \tilde{a}_Q]^T \in \mathbb{R}^Q$ 
12:     $\mathbf{b} = [b_1, b_2, \dots, b_{M_l}]^T \in \mathbb{R}^{M_l}$  obtain  $\mathbf{z}^*$  by
13:    minimize  $\|\mathbf{A}\mathbf{z} - \mathbf{b}\|_2^2$ 
14:     $\tilde{\mathbf{x}}_l = e^{j(\mathbf{A}\mathbf{z}^*)}$ 
15:     $\tilde{\mathbf{X}} = [\tilde{\mathbf{x}}_1, \tilde{\mathbf{x}}_2, \dots, \tilde{\mathbf{x}}_L]$ 
16:     $\mathbf{x}^{(i+1)} = \text{vec}(\tilde{\mathbf{X}})$ 
17:     $i \leftarrow i + 1$  return  $\mathbf{x}^{(i+1)}$ 

```

Algorithm 3 Optimal sequence with minimum ISL and polynomial phase parameters $a_{q,l}$ using MISL**Require:** N and M **Ensure:** $\mathbf{x}^{(i+1)}$

```

1: Set  $i = 0$ , initialize  $\mathbf{x}^{(0)}$ 
2: while Stopping criterion is not met do
3:    $\mathbf{f} = |\mathbf{A}^H \mathbf{x}^{(i)}|^2$ 
4:    $f_{\max} = \max(\mathbf{f})$ 
5:    $\mathbf{y}^{(i)} = -\mathbf{A} (\text{Diag}(\mathbf{f}) - f_{\max} \mathbf{I} - N^2 \mathbf{I}) \mathbf{A}^H \mathbf{x}^{(i)}$ 
6:    $\mathbf{x}^{(i+1)} = \text{PECS}(\mathbf{y}^{(i)}, L, M_l, a_{\{q,l\}}^{(i)})$ 
7: return  $\mathbf{x}^{(i+1)}$ 

```

where $\mathbf{a}_g^* = [e^{-j\omega_g}, \dots, e^{-j2N\omega_g}]$ and \mathbf{A}^* is the following unitary $2N \times 2N$ Discrete Fourier Transform (DFT) matrix

$$\mathbf{A}^* = \frac{1}{\sqrt{2N}} \begin{bmatrix} \mathbf{a}_1^* \\ \vdots \\ \mathbf{a}_{2N}^* \end{bmatrix} \quad (27)$$

$\bar{\mathbf{x}}$ is the sequence $\{x_n\}_{n=1}^N$ padded with N zeros, i.e. $\bar{\mathbf{x}} = [x_1, \dots, x_N, 0, \dots, 0]_{2N \times 1}^T$ and $\mathbf{v} = \frac{1}{\sqrt{2}} [e^{j\psi_1}, \dots, e^{j\psi_{2N}}]^T$. For given $\{x_n\}$, CAN minimizes (26) by alternating the optimization between $\bar{\mathbf{x}}$ and \mathbf{v} . Let $\bar{\mathbf{x}}^{(i)} = [x_1^{(i)}, \dots, x_N^{(i)}, 0, \dots, 0]_{2N \times 1}^T$, and let D_i represent the value of $\|\mathbf{A}^* \bar{\mathbf{x}}^{(i)} - \mathbf{v}^{(i)}\|$ at iteration i . Then we have $D_{i-1} \geq D_i$. Further in the i^{th} iteration, the objective can be minimized using the technique proposed for solving (12) by assuming

$$\begin{aligned} \mathbf{x} &= \bar{\mathbf{x}}^{(i)}, \\ \mathbf{y} &= e^{j \arg(\mathbf{d})} \end{aligned} \quad (28)$$

where $\mathbf{d} = \mathbf{A}\mathbf{v}$ denotes the inverse FFT of \mathbf{v} . The details of the implementation can be found in Algorithm 4.

Algorithm 4 Optimal sequence with minimum ISL and polynomial phase parameters $a_{q,l}$ using CAN**Require:** N and M **Ensure:** $\mathbf{x}^{(i+1)}$

```

1: Set  $i = 0$ , initialize  $\mathbf{x}^{(0)}$ .
2: while Stopping criterion is not met do
3:    $\mathbf{f} = \mathbf{A}^H \mathbf{x}^{(i)}$ 
4:    $v_g = e^{j(\arg(f_g))}, g = 1, \dots, 2N$ 
5:    $\mathbf{d} = \mathbf{A}\mathbf{v}$ 
6:    $y_n^{(i+1)} = e^{j(\arg(d_n))}, n = 1, \dots, N$ 
7:    $\tilde{\mathbf{X}} = \text{PECS}(\mathbf{y}^{(i)}, L, M_l, a_{\{q,l\}}^{(i)})$ 
8:    $\mathbf{x}^{(i+1)} = \text{vec}(\tilde{\mathbf{X}})$ 
9: return  $\mathbf{x}^{(i+1)}$ 

```

IV. PERFORMANCE ANALYSIS

In this section, we assess the performance of the proposed PECS algorithm⁷ and compare it with prior work in the literature. We then emphasize its potential to design sequences for various automotive radar applications while considering the effects of Doppler and interference.

A. ℓ_p Norm Minimization

At first, we evaluate the performance of the proposed Algorithm-1 in terms of ℓ_p norm minimization by several examples. For the initialization, we chose a random seed sequence and $Q = 2$.

Figure 3 shows the convergence behaviour of the proposed algorithm when the simulation is mandatorily run for 10^6 iterations. We chose different values of p (i.e. 2, 5, 10, 100 and $1e3$) as an input parameter of the Algorithm-1, these allow to trade-off between good PSL and ISL. For this figure, we keep the values of sequence length, sub-sequence length and polynomial degree fixed, by setting $N = 300$, $M = 5$, and $Q = 2$. Nevertheless, we observed similar behaviour in the convergence for the different values of N , M , and Q .

As evident from the Figure 3, the objective function is reduced rapidly for $p = 2$ and this rate reduces with the objective saturating after 10^5 iterations. Whereas, by increasing the value of p to 5, 10 and 100, we achieve similar convergence rate as observed earlier. Uniquely, while computing the ℓ_{1000} norm⁸, the objective converges slowly and continues to decrease until 10^6 iterations.

Further, while analysing the autocorrelation sidelobes in Figure 3 for the same set of input parameters of p, N, M and maximum number of iterations, we numerically observe that the lowest PSL values⁹ are observed for ℓ_{10} norm and other PSL values are higher for $p \neq 10$.

In Figure 4, we assess the relationship of Polynomial phase of degree Q as a tuning parameter with PSL and ISL. The parameter Q , can be considered as another degree of freedom

⁷Source code is available at "https://github.com/robin-amar/ResearchPapers/blob/eb83e644c164ac998bac7820268ee5929563583e/PECS.m"

⁸Computationally, we cannot use $p = \infty$, but by setting p to a tractable value, e.g., $p \geq 10$, we find that the peak sidelobe is effectively minimized.

⁹PSL_{dB} $\triangleq 10 \log_{10}(\text{PSL})$, ISL_{dB} $\triangleq 10 \log_{10}(\text{ISL})$.

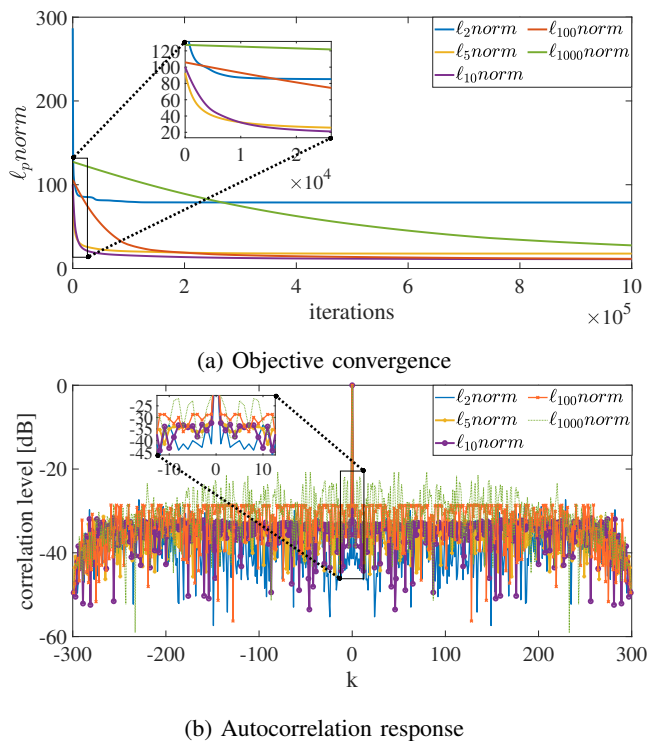


Figure 3: ℓ_p norm convergence and Autocorrelation comparison with varying p in ℓ_p norm for a sequence with input parameters $N = 300, M = 5, Q = 2$ and iterations = 10^6 .

available for the design problem. Other input parameters are kept fixed (i.e. $N = 300$ and $M = 5$) and same seed sequence is fed to the algorithm. As the value of Q is increased, we observe a decrement in the optimal PSL and ISL values generated from PECS for different norms (i.e. $p = 2, 5, 10, 100$ and 10^3). Therefore, the choice of the input parameters would vary depending upon the application.

B. Shaping the Ambiguity Function

In Table (II), we show the capability and effectiveness of the PECS algorithm to shape the AF by changing the input parameters. For the plots shown here, the input parameters are $N = 300$, varying sub-sequence lengths of $M = 5, 50, 150$ and 300 , $Q = 2$ and p limited to $2, 10$ and 100 . In the unwrapped phase plots of the sequences, the quadratic nature of the sub-sequence is retained for all values of M and p . As evident, the AF achieves the thumbtack type shape for $M = 5$ keeping quadratic behaviour in its phase and as the value of M increases, it starts evolving into a ridge-type shape. For $M = N = 300$ (i.e. only one sub-sequence, $L = 1$), it achieves a perfect ridge-shaped AF. Further, the sharpness of the ridge-shape is observed as the value of p increases (i.e. $p = 10, 100$).

C. Doppler Tolerance Evaluation

In Figure 5, we compare the Doppler tolerance characteristics of sequences: Frank, Golomb, Random and PECS with length $N = 100$. In the automotive case study considered

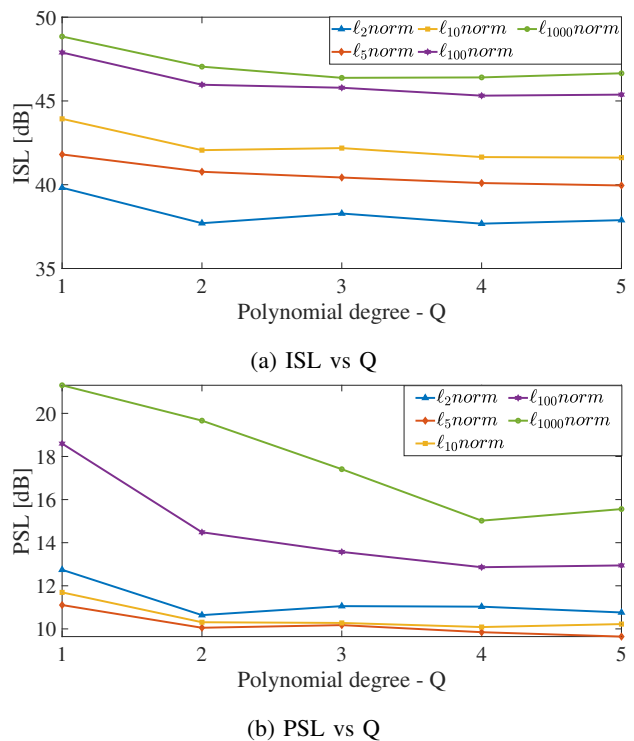
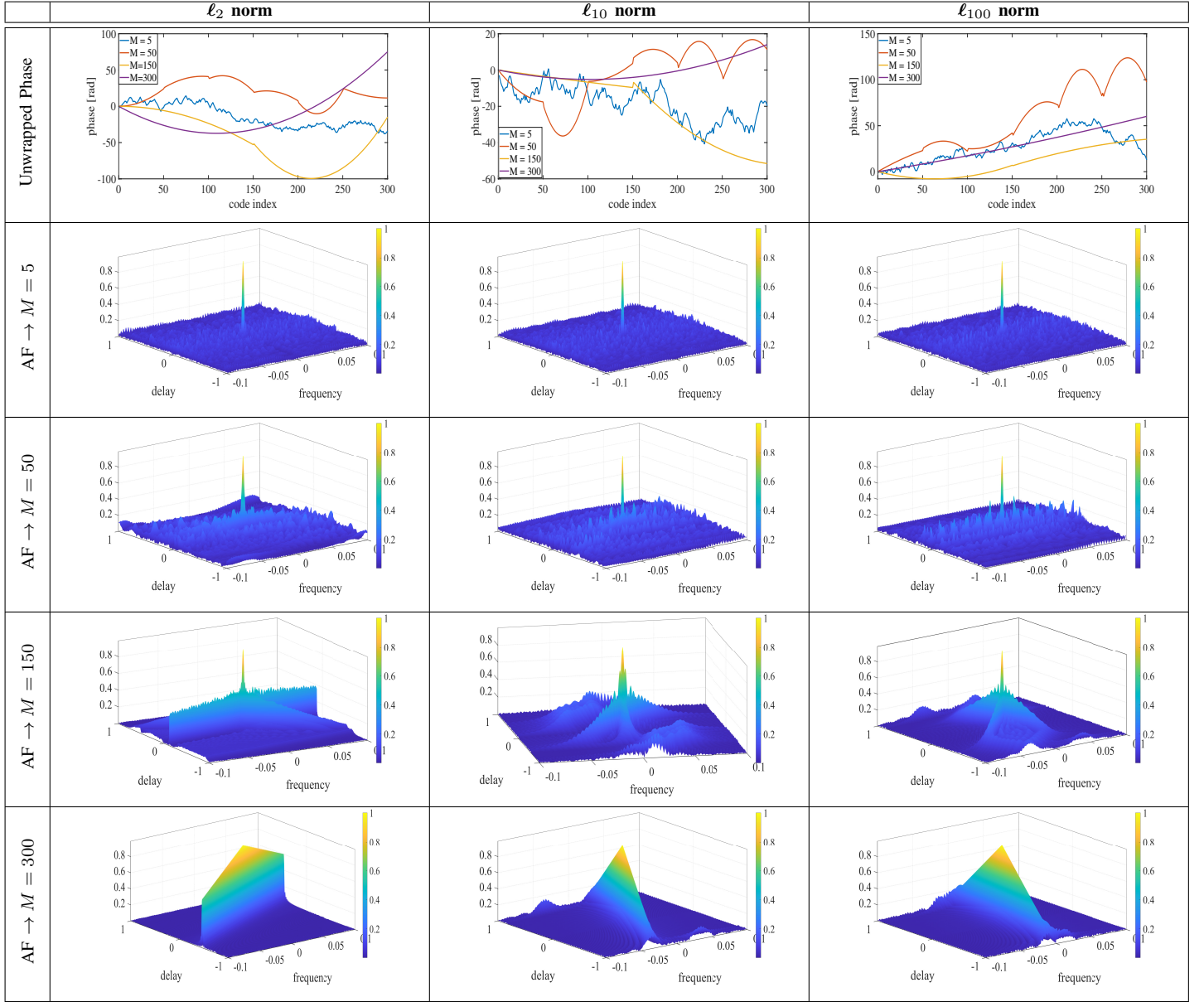


Figure 4: ISL and PSL variation with increasing Q .

in this paper, the maximum expected Doppler frequency for a radar operating at 79GHz from the targets cruising at the highest absolute relative velocity of 400kmph is roughly 58KHz. By considering range resolution of 1m (or equivalently 150MHz bandwidth), this Doppler frequency is less than 1% of the transmit signal bandwidth. Therefore for a single chirp time period the normalized Doppler frequency range of interest shown in the figure is limited to 0.01Hz. In PECS algorithm, the input parameters are: polynomial degree, $Q = 2$ and the sub-sequence length, M varies with a relation: $\{5 \leq M \leq 100\}$ and the variations in the peak amplitude of the autocorrelation as a function of normalized Doppler are shown in Figure 5a. As is evident from the plot, the peak of the matched filter decays for all the sequences as the Doppler shift increases due to target motion. But, a sharp decay of the peak value is observed in the case of Random sequence as compared to a Golomb sequence where the decay is rather linear in manner. In relation to these when the sequence is generated using PECS, and $M = N = 100$, its response is better than Frank sequence and similar to Golomb sequence. Further, as we decrease M , we observe that the Doppler shift impacts the peak and the response starts resembling the Random sequence for $M = 5$. Similar conclusions can be drawn from the Figure 5c where Integrated Sidelobe Level Ratio (ISLR) values of various sequences are observed. Further, the correlation level, Peak Sidelobe Level Ratio (PSLR) and the ISLR variation with normalized Doppler is shown in Figure 5b

Table II: Unwrapped phase and Ambiguity Function comparison for $N = 300$, $Q = 2$, $M \in [5, 50, 150, 300]$ and $p \in [2, 10, 100]$ in ℓ_p norm.


and Figure 5c respectively.

$$\begin{aligned}
 \text{correlation level} &\triangleq \left| \frac{r_k}{r_0} \right|, \\
 \text{PSLR}_{dB} &\triangleq 20 \log_{10} \frac{\text{PSL}}{\max\{|r_k|\}_{k=0}^{N-1}}, \\
 \text{ISLR}_{dB} &\triangleq 20 \log_{10} \frac{\text{ISL}}{\max\{|r_k|\}_{k=0}^{N-1}}
 \end{aligned} \quad (29)$$

On the other hand, as the number of sub-sequences increase in the PECS sequences (e.g "PECS M25" and "PECS M5") the PSL begins to rise and eventually lowers the PSLR. This may impact the detection probability of the target.

D. Comparison with the Counterparts

1) *Performance*: In [42], an approach was presented for designing polyphase sequences with piecewise linearity and impulse like autocorrelation properties (further referred as "LinearPhaseMethod"). In order to compare the performance of the LinearPhaseMethod with the proposed PECS, we use both the algorithms to design a piecewise linear polyphase sequence of length $N = 128$ with sub-sequence length 8 and thereby the total number of sub-sequences are 16. Normalized autocorrelation of the optimized sequences from both the approaches is shown in Figure 6a and it shows lower PSL values of the autocorrelation for PECS as compared to LinearPhaseMethod. Unwrapped phase of the optimized

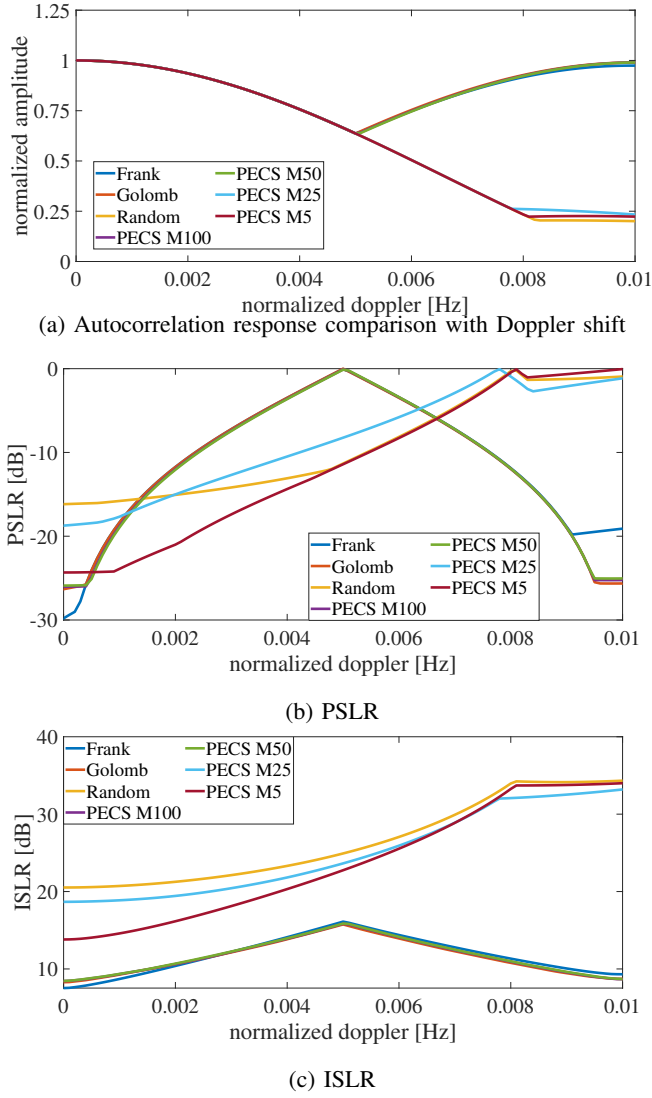


Figure 5: Comparison of various sequences for evaluating the Doppler tolerance

sequences are shown in Figure 6b¹⁰. Linear Phase Method generates an optimal sequence whose ISL and PSL values are 36.47dB and 12.18dB respectively whereas PECS results in an optimal sequence whose ISL and PSL values are 32.87dB and 9.09dB. Therefore, better results are obtained using PECS approach.

In [38], an approach to shape the AF of a given sequence w.r.t. a desired sequence was proposed (later referred as "AF shape method"). Here, we consider an example where the two approaches (i.e. AF shaping method and PECS) strive to achieve the desired AF of a Golomb sequence of length $N = 64$. The performance of the two approaches would be assessed by comparing the autocorrelation responses and ISL/PSL values of the optimal sequences. Both the algorithms

¹⁰the phase unwrapping operation can be expressed mathematically as

$$\mathbf{x}_U = \mathcal{F}[\mathbf{x}_W] = \arg(\mathbf{x}_W) + 2k\pi$$

where \mathcal{F} is the phase unwrapping operation, k is an integer, \mathbf{x}_W and \mathbf{x}_U are the wrapped and unwrapped phase sequence, respectively

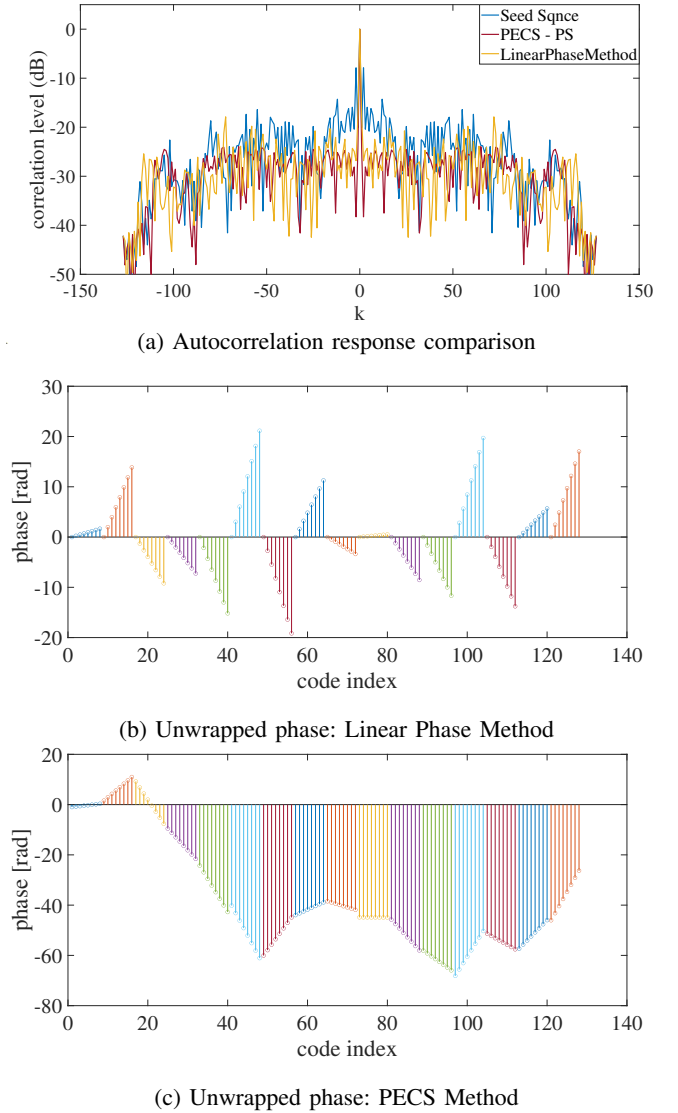
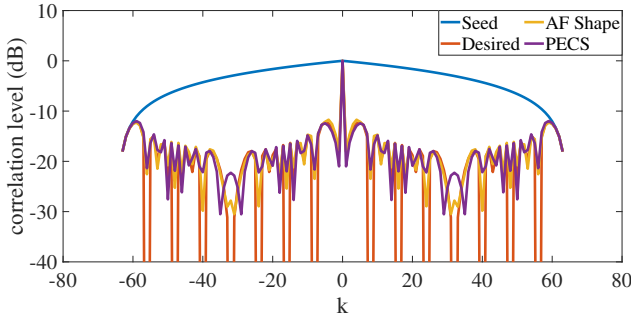


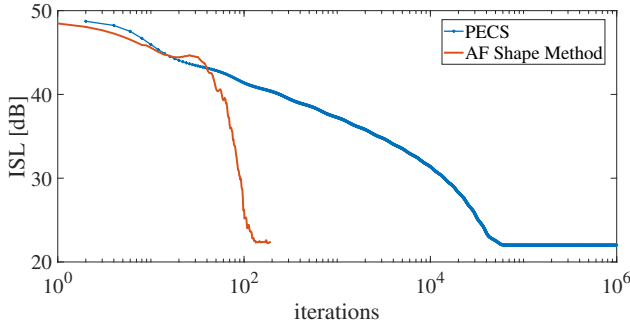
Figure 6: Comparison of Linear Phase Method and PECS to design linear polyphase sequence with good autocorrelation properties.

are fed with the same seed sequence and the convergence criterion is kept the same for better comparison. As evident from the Figure 7, the autocorrelation function of the optimal sequence derived from PECS shows improvement as compared to the optimal sequence of benchmark approach. The initial ISL of the seed sequence was 49.30dB and the desired Golomb sequence was 22.050dB. After the optimization was performed, the optimal ISL using AF shaping approach was 22.345dB and using PECS was 22.002dB. In addition, the ridge shape of the AF generated using both the approaches is equally matched to the desired AF of Golomb sequence. Noteworthy point over here is that the monotonic convergence is absent in the AF shape method as it optimizes using the CD approach whereas in the PECS method, monotonic convergence is achieved. Further, PECS has the capability of achieving better ISL values than the Golomb sequence as it aims to minimize the objective in (8) and its proof can be

seen from the optimal ISL value quoted above (i.e. 0.048dB improvement w.r.t. ISL of Golomb sequence).



(a) Autocorrelation response comparison



(b) ISL Convergence: PECS Method

Figure 7: Performance comparison of AF Shape method and PECS algorithms.

2) *Run-time*: To calculate run-time of the algorithm we used a PC with the following specifications: 2.6GHz i9 – 11950H CPU and 32GB RAM. No acceleration schemes (i.e. Parallel Computing Toolbox in MATLAB) are used to generate the results and are evaluated from purely sequential processing.

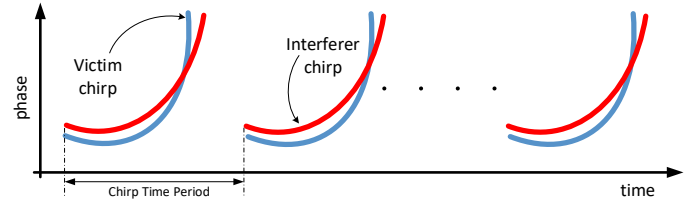
For a sequence length of $N = 300$, computational time was derived by varying two input parameters: sub-sequence length $M = 5, 50, 150$ & 300 and $Q = 2, 3, 4, 5$ & 6 . The results mentioned in Table III indicate that the computation time increases in proportion to the increasing values of Q keeping M fixed. On the other hand, computation time decreases as we keep Q fixed and increase M .

Table III: PECS runtime - sequence length $N = 300$

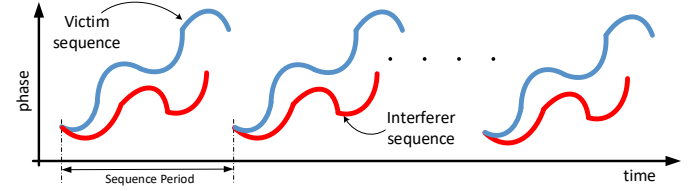
	$M=5$	$M=50$	$M=150$	$M=300$
$Q=2$	429.25s	84.26s	52.53s	45.15s
$Q=3$	521.41s	88.32s	55.03s	47.42s
$Q=4$	562.04s	97.20s	64.55s	56.54s
$Q=5$	573.72s	108.37s	73.47s	65.47s
$Q=6$	620.90s	118.82s	83.39s	74.06s

E. Automotive Scenario

The idea is to generate a code sequence using PECS algorithm towards designing a transmission scheme for PMCW and evaluate its performance by comparing it with the FMCW waveform transmission when interference is introduced in the



(a) Quadratic phase FMCW waveform



(b) PECS based PMCW waveform

Figure 8: Phase variation comparison of FMCW and PMCW waveform.

FoV of the victim sensor. Figure 8 shows the phase-time plot comparison of both the waveforms. In this plot, the pulse length, T_p (i.e. chirp time period - FMCW and sequence period - PMCW) and pulse repetition frequency (PRF), f_p of both the type of waveforms is matched for simplicity of the concept which results in equal Doppler response of the target. PECS code sequence has input parameters: quadratic phase $Q = 2$, code length $N = \frac{T_p}{\tau_{chirp}}$ and varying sub-sequence length M . Thus, the MI occurs within a single pulse time period T_p amongst FMCW waveforms but it is less likely going to occur in PECS waveforms. Even though the initial phase in FMCW waveform from two different sensors would start from any random initialization, they tend to interfere as they exhibit similar quadratic phase behavior for the whole chirp time. This phenomenon is not seen in PECS waveforms since any sensor can choose different sub-sequence lengths and hence result in different quadratic phase coefficients resulting in minimal cross-correlation with other transmitting sequences in its FoV.

In Figure 9 few automotive scenarios are described where MI may occur. As mentioned in the introduction, two types of interference are witnessed using FMCW i.e. Similar-slope and sweeping slope interference. The similar-slope interference occurs when the sensors operate with same specifications in order to sense the environment for the following applications:

- whenever a sensor is mounted for Blind Spot Detection (BSD) application in ego-vehicle Figure 9a and another vehicle with Short Range Radar (SRR) mounted on front side enters the FoV.
- when the ego vehicle is equipped with Adaptive Cruise Control (ACC) function, it follows the trajectory of a car driving ahead. The target vehicle may be equipped with a rear mounted radar and would lie in the FoV of the front mounted radar on the ego vehicle Figure 9c.
- Front side mounted radar from the Ego-Vehicle may get interfered by another overtaking vehicle equipped with a rear side mounted radar Figure 9d.

In Figure 9b, Sweeping slope interference may occur when a side looking radar of the oncoming target vehicle is in the

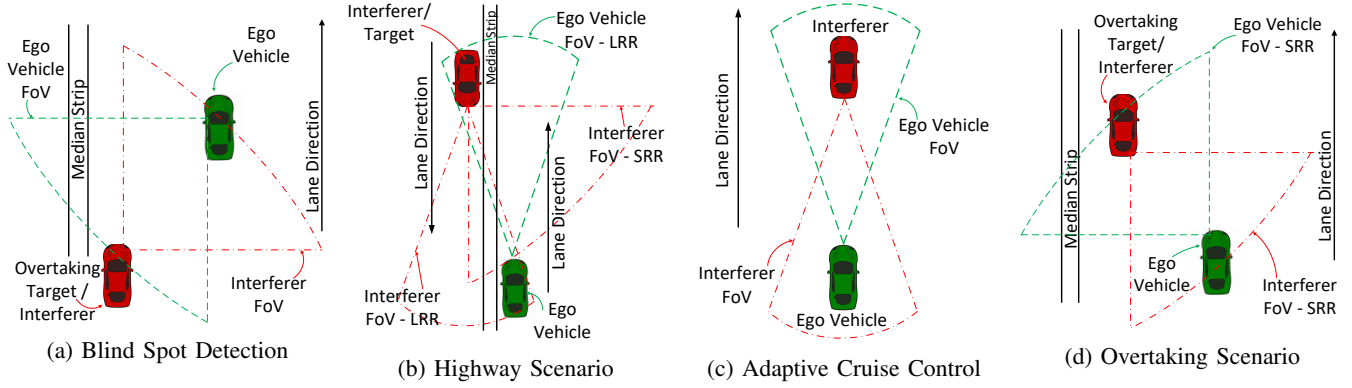


Figure 9: Automotive scenarios with mutual interference.

FoV of the ego vehicle's front looking radar, provided both are operating in the same band (i.e. 77 – 81GHz).

1) *Simulation results:* To demonstrate the efficacy of the proposed algorithm, we simulated an automotive driving scenario for the cases described in Figure 9. Here, radar sensing performance was evaluated independently in two different cases:

- when the ego-vehicle is operating with FMCW waveform and MI (i.e. similar-slope and sweeping slope) is observed from the target.
- the ego-vehicle is operating with PMCW waveform using PECS algorithm based code sequence and encounters MI from another target in its FoV with the same scheme.

Table IV: Radar sensor parameters and Motion information for ego-vehicle and interfering vehicle

	parameter	value
FMCW & PMCW params	Operating Frequency	79GHz
	Antenna Gain	10dB
	Range Resolution	1m
	Transmit Power (Victim / Interferer)	12dBm
	Bandwidth (Victim)	150 MHz
	Bandwidth (Sweeping-slope Interferer)	75 MHz
	Bandwidth (Similar-slope Interferer)	148.5 MHz
	Pulse length (T_p)	60 us
	PRF (f_p)	16.66 kHz
	Number of Pulses	256
	Chip Time	6.66 ns
	Code Length	4500
Motion Info	Target Range	30m
	Target Speed	20kmph
	Target RCS	10dBsm
	Interferer Range	50m
	Interferer Speed	40kmph

The radar sensing parameters for both the FMCW and PMCW waveforms are described in the Table IV. In order to have a fair comparison, we have matched the time bandwidth product (TBP) and Doppler characteristics (pulse length, PRF) of both the waveforms. Figure 10 shows the comparison of the range-Doppler map for similar-slope and sweeping slope interference in FMCW and PMCW waveforms. In FMCW waveforms, the Signal to Interference plus Noise Ratio (SINR) of the victim sensor in an interference free scenario is 13.06dB. When a single interferer is introduced,

the similar-slope interference observed by the victim-sensor (driving scenarios mentioned previously in Figure 9a, 9c & 9d) witnessed a SINR of 10.8dB (refer Figure 10a). Similarly with single interferer, in the case of sweeping slope interference Figure 10b the SINR was 12.9dB. Although, these results have been derived after applying mitigation technique (i.e. varying PRF at the victim sensor), the impact of interference on the detection capability of the victim sensor is evident and weak targets may not be detected in such a scenario. In the current case, the target, interferer position and Doppler have been deliberately kept different for purposes of plotting but if both have similar values, the detectability of target becomes even more arduous in the case of similar-slope interference.

On the other hand for PMCW waveform derived from PECS, both the victim and the interferer sensor transmit an optimized PECS code sequence which is Doppler tolerant and unique. Noteworthy fact here is that both the victim and interferer are operating at the same bandwidth (i.e. same range resolution), center frequency and transmit power without causing MI which proves the robustness of algorithm. As is evident from Figure 10c, there is no interference peak present in the range-Doppler spectrum and the SINR in the case of single interferer is 20.7dB better than FMCW in interference free scenario. Further to this result, the reduction in the SINR due to increase in the number of interferers was analyzed. The results from the simulation show that as the number of interferers increase from one to five, the SINR decreases to 16.8dB. As the presence of more than 10 interferers in a certain driving scenario is very unlikely, therefore the interference results were limited to 10 interferers and SINR in this case was 14.65dB.

The spectrum occupancy of FMCW and PECS based PMCW waveform is mentioned in Figure 10d and Figure 10e. We observed that in the duration of single chirp (where chirp time period = sequence period), the frequency variation of FMCW waveform is linearly increasing upto 150MHz whereas in PECS waveform multiple ramps of linearly increasing frequency can be seen in the time period. This again ascertains the fact that the frequency variation is linear (hence the quadratic phase variation). Randomness in the ramp slopes within a chirp duration and start phase is the reason for the uniqueness of each waveform and can be considered as

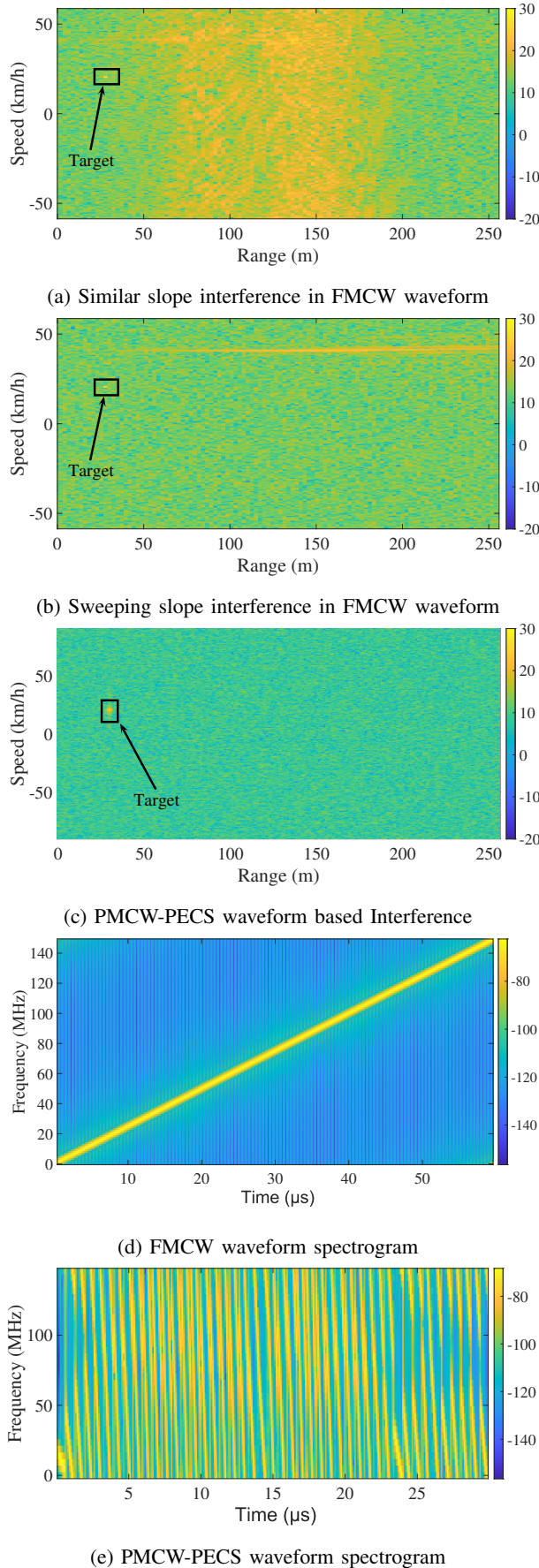


Figure 10: scenario with FMCW and PMCW type waveforms being used by the Ego-Vehicle and target respectively (Power values on *colorscale* are in dBm).

an additional degree of freedom in the system design which leads to interference immune waveform. Thus, PECS can be considered a new approach in this domain.

2) *Statistical Analysis:* Further, in order to understand the interference immunity of different waveforms, a statistical validation of this concept was performed and its comparison was evaluated. In the first category, two independent sequences with same properties ($N = 100$, $M = 10$, $Q = 3$ and $p = 10$) were generated using PECS algorithm. In the second and third category, two independent sequences were designed with such characteristics that they cause similar-slope and sweeping slope FMCW interference, respectively. A statistical analysis of maximum cross-correlation was performed for 10^3 trials and the results are given in Figure 11 for each of the category. The x -axis represents normalized cross-correlation of two signals and the y -axis represents the probability of occurrence in 10^3 trials. As the PECS framework allows additional degree of freedom in choosing the sub-sequence length randomly, the analysis for the PECS category was performed with $M \in [M_{min}, M_{max}]$ where $M_{min} = 5$ and $M_{max} = 20$. This category does not impact the performance of the maximum cross-correlation and is similar to the one which can be achieved if two completely random sequences are correlated. The cross correlation results obtained from similar-slope and sweeping slope interference are centered at -1.5 dB and -0.2 dB respectively, whereas for PECS based sequences cross-correlation is centered at -14.1 dB. As is evident from the plot, an improvement of approximately 12dB is expected if PMCW waveform with PECS based code sequences are used for radar sensing as compared to the FMCW waveform. This proves the credibility and robustness of the concept.

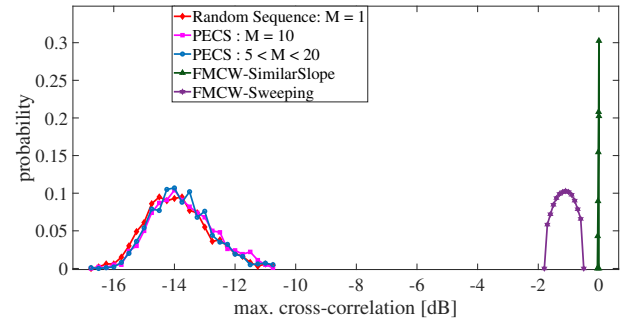


Figure 11: Statistical Interference Analysis - Probabilistic comparison of code sequences of length $N = 100$ generated using (a) PECS with fixed length sub-sequences $M = 10$ (b) PECS with random length sub-sequences $M_{min} = 5$ and $M_{max} = 20$ (c) completely random sequence.

V. CONCLUSION

A stable design procedure has been proposed for obtaining polyphase sequences synthesized with a constraint of polynomial phase behavior optimized for minimal PSL/ISL for any sequence length. Results shown in the text indicate the robustness of the method for various scenarios which are prone to interference and offers user additional degrees of

freedom to adapt the input parameters in order to design unique waveforms. Its application to automotive scenarios with dense interference prove the feasibility of its use in practical radar systems and provides one of the solution to the current interference issues in multi-sensor applications. The algorithm performance was tested in comparison to the other techniques present in the literature and convincing results were observed. In addition the technique can be used to improve the performance of the state-of-the-art algorithms by extending them with inclusion of PECS which offers additional design parameters for waveform design. The algorithm is implemented by means of FFT and least squares operations and therefore it is computationally efficient.

APPENDIX A CHIRPLIKE PHASE CODES

A summary of chirplike phase codes is reported in Table V. Note that Frank code is derived from the phase history of a linearly frequency stepped pulse. The main drawback of the Frank code is that it only applies for codes of perfect square length ($M = L^2$) [23]. P1, P2, and Px codes are all modified versions of the Frank code, with the DC frequency term in the middle of the pulse instead of at the beginning. Unlike Frank, P1, P2 and Px codes which are only applicable for perfect square lengths ($M = L^2$), the Zadoff code is applicable for any length.

Chu codes are important variant of the Zadoff code, and Golomb, P3, and P4 codes are specific cyclically shifted and decimated versions of the Zadoff-Chu code. Indeed, as P1 and P2/Px codes were linked to the original Frank code, similarly, P3, P4 and Golomb polyphase codes are linked to the Zadoff-Chu code, and are given for any length.

APPENDIX B DERIVATION OF MM-PSL

We aim to obtain a minimizer of (8) iteratively using MM algorithm. We can majorize $|r_k|^p$ by a quadratic function locally [27]. From the literature (see [27], [28] for more details), it is known that given $|r_k^{(i)}|$ at iteration i , $|r_k|^p$ can be majorized at $|r_k^{(i)}|$ over $[0, t]$ by

$$\tilde{\alpha}_k |r_k|^2 + \tilde{\beta}_k |r_k| + \tilde{\alpha}_k \left| r_k^{(i)} \right|^2 - (p-1) \left| r_k^{(i)} \right|^p, \quad (30)$$

where

$$t = \left(\sum_{k=1}^{N-1} |\tilde{r}_k^{(i)}|^p \right)^{\frac{1}{p}}$$

$$\tilde{\alpha}_k = \frac{t^p - \left| r_k^{(i)} \right|^p - p \left| r_k^{(i)} \right|^{p-1} (t - \left| r_k^{(i)} \right|)}{(t - \left| r_k^{(i)} \right|)^2}, \quad (31)$$

$$\tilde{\beta}_k = p \left| r_k^{(i)} \right|^{p-1} - 2\tilde{\alpha}_k \left| r_k^{(i)} \right|.$$

The surrogate function is then given by (ignoring the constant terms)

$$\sum_{k=1}^{N-1} (\tilde{\alpha}_k |r_k|^2 + \tilde{\beta}_k |r_k|) \quad (32)$$

The first term in the objective function is just the weighted ISL metric with weights $w_k = \tilde{\alpha}_k$, which can be majorized at $\mathbf{x}^{(i)}$ by (with constant terms ignored) [27]

$$\mathbf{x}^H \left(\mathbf{R} - \lambda_{\max}(\mathbf{L}) \mathbf{x}^{(i)} (\mathbf{x}^{(i)})^H \right) \mathbf{x}, \quad (33)$$

$$\mathbf{R} = \sum_{k=1}^{N-1} w_k r_k^{(i)} \mathbf{U}_k, \quad \mathbf{L} = \sum_{k=1}^{N-1} w_k \text{vec}(\mathbf{U}_k) \text{vec}(\mathbf{U}_k)^H,$$

$$\lambda_{\max}(\mathbf{L}) = \max_k \{w_k (N-k) |k=1, \dots, N-1\},$$

and \mathbf{U}_k , $k=0, \dots, N-1$ to be $N \times N$ Toeplitz matrix with the k -th diagonal elements being 1 and 0 elsewhere. For the second term, since it can be shown that $\tilde{\beta}_k \leq 0$, we have

$$\sum_{k=1}^{N-1} \tilde{\beta}_k |r_k| \leq \frac{1}{2} \mathbf{x}^H \left(\sum_{k=1}^{N-1} \tilde{\beta}_k \frac{r_k^{(i)}}{|r_k^{(i)}|} \mathbf{U}_{-k} \right) \mathbf{x}. \quad (34)$$

By adding the two majorization functions, i.e. (33) and (34), and other simplifications as given in [27], we derive the majorizer of (32) as

$$\mathbf{x}^H \left(\tilde{\mathbf{R}} - \lambda_{\max}(\mathbf{L}) \mathbf{x}^{(i)} (\mathbf{x}^{(i)})^H \right) \mathbf{x} \quad (35)$$

where $\hat{w}_{-k} = \hat{w}_k = \tilde{\alpha}_k + \frac{\tilde{\beta}_k}{2|r_k^{(i)}|} = \frac{p}{2} |r_k^{(i)}|^{p-2}$, $k=1, \dots, N-1$ and $\tilde{\mathbf{R}} = \sum_{k=1}^{N-1} \hat{w}_k r_k^{(i)} \mathbf{U}_k$. Finally, after performing one more majorization step as mentioned in [27], we derive another majorizer as

$$\|\mathbf{x} - \mathbf{y}\|_2 \quad (36)$$

where $\mathbf{y} = (\lambda_{\max}(\mathbf{L})N + \lambda_u) \mathbf{x}^{(i)} - \tilde{\mathbf{R}} \mathbf{x}^{(i)}$, which forms the basis of our problem in (12).

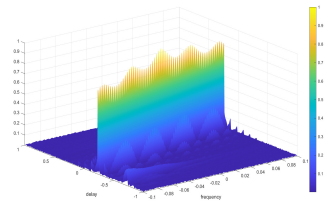
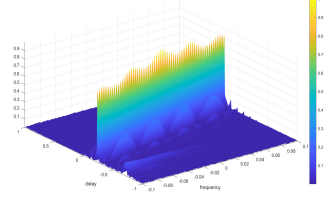
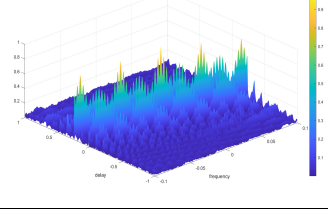
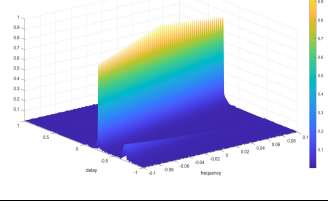
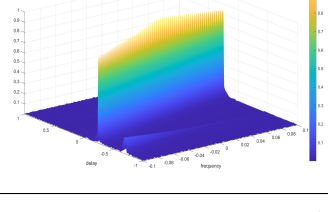
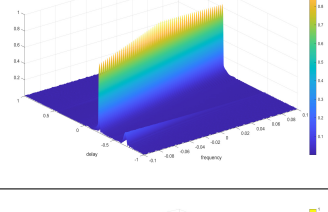
REFERENCES

- [1] J. Hasch, E. Topak, R. Schnabel, T. Zwick, R. Weigel, and C. Waldschmidt, "Millimeter-wave technology for automotive radar sensors in the 77 ghz frequency band," *IEEE Transactions on Microwave Theory and Techniques*, vol. 60, no. 3, pp. 845–860, 2012.
- [2] S. M. Patole, M. Torlak, D. Wang, and M. Ali, "Automotive radars: A review of signal processing techniques," *IEEE Signal Processing Magazine*, vol. 34, no. 2, pp. 22–35, 2017.
- [3] G. Wang, C. Gu, T. Inoue, and C. Li, "A hybrid fmcw-interferometry radar for indoor precise positioning and versatile life activity monitoring," *IEEE Transactions on Microwave Theory and Techniques*, vol. 62, no. 11, pp. 2812–2822, 2014.
- [4] S. Chen, C. Luo, B. Deng, Y. Qin, H. Wang, and Z. Zhuang, "Research on characteristics of rough and smooth pedestrian in terahertz band," in *2016 41st International Conference on Infrared, Millimeter, and Terahertz waves (IRMMW-THz)*, 2016, pp. 1–2.
- [5] G. Beltrão, M. Alaei-Kerahroodi, U. Schroeder, and M. Bhavani Shankar, "Joint waveform/receiver design for vital-sign detection in signal-dependent interference," in *2020 IEEE Radar Conference (RadarConf20)*, 2020, pp. 1–6.
- [6] S. Rao and A. V. Mani, "Interference characterization in fmcw radars," in *2020 IEEE Radar Conference (RadarConf20)*, 2020, pp. 1–6.
- [7] R. Amar, M. Alaei-Kerahroodi, and M. R. Bhavani Shankar, "Fmcw-interference analysis in mm-wave radars; an indoor case study and validation by measurements," in *2021 21st International Radar Symposium (IRS)*, 2021, pp. 1–11.
- [8] M. A. Richards, J. Scheer, W. A. Holm, and W. L. Melvin, *Principles of modern radar*. Citeseer, 2010.
- [9] H. Rohling and M.-M. Meinecke, "Waveform design principles for automotive radar systems," in *2001 CIE International Conference on Radar Proceedings (Cat No.01TH8559)*, 2001, pp. 1–4.
- [10] M. Jankiraman, *FMCW Radar Design*. Artech House, 2018.

- [11] J. J. de Witt and W. A. Nel, "Range doppler dynamic range considerations for dechirp on receive radar," in *2008 Euro. Radar Conf.*, 2008, pp. 136–139.
- [12] Y. Al-Alem, L. Albasha, and H. Mir, "High-resolution on-chip s -band radar system using stretch processing," *IEEE Sensors Journal*, vol. 16, no. 12, pp. 4749–4759, 2016.
- [13] Z. Tong, R. Renter, and M. Fujimoto, "Fast chirp FMCW radar in automotive applications," in *IET Intl. Radar Conf.*, 2015, pp. 1–4.
- [14] J. J. Benedetto, I. Konstantinidis, and M. Rangaswamy, "Phase-coded waveforms and their design," *IEEE Signal Processing Magazine*, vol. 26, no. 1, pp. 22–31, 2009.
- [15] A. Bourdoux, U. Ahmad, D. Guermandi, S. Brebels, A. Dewilde, and W. Van Thillo, "PMCW waveform and MIMO technique for a 79 GHz CMOS automotive radar," in *2016 IEEE Radar Conference (RadarConf)*, 2016, pp. 1–5.
- [16] N. Levanon and B. Getz, "Comparison between linear fm and phase-coded cw radars," *IEE Proceedings-Radar, Sonar and Navigation*, vol. 141, no. 4, pp. 230–240, 1994.
- [17] J. Overvest, F. Jansen, F. Uysal, and A. Yarovoy, "Doppler influence on waveform orthogonality in 79 ghz mimo phase-coded automotive radar," *IEEE Transactions on Vehicular Technology*, vol. 69, no. 1, pp. 16–25, 2020.
- [18] R. Frank, "Polyphase codes with good nonperiodic correlation properties," *IEEE Transactions on Information Theory*, vol. 9, no. 1, pp. 43–45, 1963.
- [19] B. L. Lewis and F. F. Kretschmer, "Linear frequency modulation derived polyphase pulse compression codes," *IEEE Transactions on Aerospace and Electronic Systems*, vol. AES-18, no. 5, pp. 637–641, 1982.
- [20] N. Zhang and S. Golomb, "Polyphase sequence with low autocorrelations," *IEEE Transactions on Information Theory*, vol. 39, no. 3, pp. 1085–1089, 1993.
- [21] D. Chu, "Polyphase codes with good periodic correlation properties (corresp.)," *IEEE Transactions on Information Theory*, vol. 18, no. 4, pp. 531–532, 1972.
- [22] D. Petrolati, P. Angeletti, and G. Toso, "New piecewise linear polyphase sequences based on a spectral domain synthesis," *IEEE Transactions on Information Theory*, vol. 58, no. 7, pp. 4890–4898, 2012.
- [23] M. E. Levanon Nadav, *Radar Signals*. John Wiley & Sons, Inc., Publication, 2004.
- [24] A. Rihaczek, "Doppler-tolerant signal waveforms," *Proceedings of the IEEE*, vol. 54, no. 6, pp. 849–857, 1966.
- [25] P. Stoica, J. Li, and M. Xue, "Transmit codes and receive filters for radar," *IEEE Signal Processing Magazine*, vol. 25, no. 6, pp. 94–109, 2008.
- [26] P. Stoica, H. He, and J. Li, "New algorithms for designing unimodular sequences with good correlation properties," *IEEE Transactions on Signal Processing*, vol. 57, no. 4, pp. 1415–1425, 2009.
- [27] J. Song, P. Babu, and D. P. Palomar, "Sequence design to minimize the weighted integrated and peak sidelobe levels," *IEEE Transactions on Signal Processing*, vol. 64, no. 8, pp. 2051–2064, 2016.
- [28] M. Alae-Kerahroodi, A. Aubry, A. De Maio, M. M. Naghsh, and M. Modarres-Hashemi, "A coordinate-descent framework to design low PSL/ISL sequences," *IEEE Transactions on Signal Processing*, vol. 65, no. 22, pp. 5942–5956, Nov 2017.
- [29] J. M. Baden, B. O'Donnell, and L. Schmieder, "Multiobjective sequence design via gradient descent methods," *IEEE Transactions on Aerospace and Electronic Systems*, vol. 54, no. 3, pp. 1237–1252, 2018.
- [30] E. Raei, M. Alae-Kerahroodi, and M. B. Shankar, "Spatial- and range-ISLR trade-off in MIMO radar via waveform correlation optimization," *IEEE Transactions on Signal Processing*, vol. 69, pp. 3283–3298, 2021.
- [31] Q. Liu, W. Ren, K. Hou, T. Long, and A. E. Fathy, "Design of polyphase sequences with low integrated sidelobe level for radars with spectral distortion via majorization-minimization framework," *IEEE Transactions on Aerospace and Electronic Systems*, vol. 57, no. 6, pp. 4110–4126, 2021.
- [32] S. P. Sankuru, P. Babu, and M. Alae-Kerahroodi, "UNIPOL: Unimodular sequence design via a separable iterative quartic polynomial optimization for active sensing systems," *Signal Processing*, vol. 190, p. 108348, 2022. [Online]. Available: <https://www.sciencedirect.com/science/article/pii/S0165168421003856>
- [33] R. Jyothi, P. Babu, and M. Alae-Kerahroodi, "Slope: A monotonic algorithm to design sequences with good autocorrelation properties by minimizing the peak sidelobe level," *Digital Signal Processing*, vol. 116, p. 103142, 2021.
- [34] X. Feng, Y. nan Zhao, Z. quan Zhou, and Z. feng Zhao, "Waveform design with low range sidelobe and high doppler tolerance for cognitive radar," *Signal Processing*, vol. 139, pp. 143–155, 2017.
- [35] W.-Q. Wang, "Large time-bandwidth product mimo radar waveform design based on chirp rate diversity," *IEEE Sensors Journal*, vol. 15, no. 2, pp. 1027–1034, 2015.
- [36] J. Zhang, C. Shi, X. Qiu, and Y. Wu, "Shaping radar ambiguity function by l -phase unimodular sequence," *IEEE Sensors Journal*, vol. 16, no. 14, pp. 5648–5659, 2016.
- [37] O. Aldayel, T. Guo, V. Monga, and M. Rangaswamy, "Adaptive sequential refinement: A tractable approach for ambiguity function shaping in cognitive radar," in *2017 51st Asilomar Conference on Signals, Systems, and Computers*, 2017, pp. 573–577.
- [38] M. Alae-Kerahroodi, S. Sedighi, B. Shankar M.R., and B. Ottersten, "Designing (in)finite-alphabet sequences via shaping the radar ambiguity function," in *ICASSP 2019 - 2019 IEEE International Conference on Acoustics, Speech and Signal Processing (ICASSP)*, 2019, pp. 4295–4299.
- [39] Z.-J. Wu, Z.-Q. Zhou, C.-X. Wang, Y.-C. Li, and Z.-F. Zhao, "Doppler resilient complementary waveform design for active sensing," *IEEE Sensors Journal*, vol. 20, no. 17, pp. 9963–9976, 2020.
- [40] I. A. Arriaga-Trejo, "Design of constant modulus sequences with doppler shift tolerance and good complete second order statistics," in *2020 IEEE International Radar Conference (RADAR)*, 2020, pp. 274–279.
- [41] X. Feng, Q. Song, Z. Zhang, and Y. Zhao, "Novel waveform design with low probability of intercept and high doppler tolerance for modern cognitive radar," in *2019 IEEE International Conference on Signal, Information and Data Processing (ICSIDP)*, 2019, pp. 1–6.
- [42] M. Soltanalian, P. Stoica, M. M. Naghsh, and A. De Maio, "Design of piecewise linear polyphase sequences with good correlation properties," in *2014 22nd European Signal Processing Conference (EUSIPCO)*, 2014, pp. 1297–1301.
- [43] A. Aubry, A. De Maio, B. Jiang, and S. Zhang, "Ambiguity function shaping for cognitive radar via complex quartic optimization," *IEEE Transactions on Signal Processing*, vol. 61, no. 22, pp. 5603–5619, 2013.
- [44] L. Wu, P. Babu, and D. P. Palomar, "Cognitive radar-based sequence design via sinr maximization," *IEEE Transactions on Signal Processing*, vol. 65, no. 3, pp. 779–793, 2017.
- [45] J. Zhang and N. Xu, "Discrete phase coded sequence set design for waveform-agile radar based on alternating direction method of multipliers," *IEEE Transactions on Aerospace and Electronic Systems*, vol. 56, no. 6, pp. 4238–4252, 2020.
- [46] W. Huang and R. Lin, "Efficient design of doppler sensitive long discrete-phase periodic sequence sets for automotive radars," in *2020 IEEE 11th Sensor Array and Multichannel Signal Processing Workshop (SAM)*, 2020, pp. 1–5.
- [47] G. M. Brooker, "Mutual interference of millimeter-wave radar systems," *IEEE Transactions on Electromagnetic Compatibility*, vol. 49, no. 1, pp. 170–181, 2007.
- [48] M. Goppelt, H.-L. Blöcher, and W. Menzel, "Analytical investigation of mutual interference between automotive fmcw radar sensors," in *2011 German Microwave Conference*, 2011, pp. 1–4.
- [49] S. Alland, W. Stark, M. Ali, and M. Hegde, "Interference in automotive radar systems: Characteristics, mitigation techniques, and current and future research," *IEEE Signal Processing Magazine*, vol. 36, no. 5, pp. 45–59, 2019.
- [50] D. M. Kurnet, "Recommendations on sensor design, mounting and operational parameters to minimize radar interference," *MOSARIM*, 2012.
- [51] M. Toth, P. Meissner, A. Melzer, and K. Witrisal, "Performance comparison of mutual automotive radar interference mitigation algorithms," in *2019 IEEE Radar Conference (RadarConf)*, 2019, pp. 1–6.
- [52] S. Rao and A. Varghese Mani, "Characterization of some interference mitigation schemes in fmcw radar," in *2021 IEEE Radar Conference (RadarConf21)*, 2021, pp. 1–6.
- [53] C. Aydogdu, M. F. Keskin, G. K. Carvajal, O. Eriksson, H. Hellsten, H. Herbertsson, E. Nilsson, M. Rydstrom, K. Vanas, and H. Wymeersch, "Radar interference mitigation for automated driving: Exploring proactive strategies," *IEEE Signal Processing Magazine*, vol. 37, no. 4, pp. 72–84, 2020.
- [54] A. Bourdoux, K. Parashar, and M. Bauduin, "Phenomenology of mutual interference of FMCW and PMCW automotive radars," in *2017 IEEE Radar Conference (RadarConf)*, 2017, pp. 1709–1714.
- [55] J. Song, P. Babu, and D. P. Palomar, "Optimization methods for designing sequences with low autocorrelation sidelobes," *IEEE Transactions on Signal Processing*, vol. 63, no. 15, pp. 3998–4009, 2015.
- [56] Y. Sun, P. Babu, and D. P. Palomar, "Majorization-minimization algorithms in signal processing, communications, and machine learning," *IEEE Transactions on Signal Processing*, vol. 65, no. 3, pp. 794–816, 2017.

- [57] E. Raei, M. Alae-Kerahroodi, P. Babu, and M. R. B. Shankar, "Design of MIMO radar waveforms based on lp-norm criteria," 2021.
- [58] D. R. Hunter and K. Lange, "A tutorial on mm algorithms," *The American Statistician*, vol. 58, no. 1, pp. 30–37, 2004.
- [59] K. Lange, *MM Optimization Algorithms*. Philadelphia, PA, USA: SIAM-Society for Industrial and Applied Mathematics, 2016.
- [60] F. L. Gall and F. Urrutia, "Improved rectangular matrix multiplication using powers of the coppersmith-winograd tensor," in *Proceedings of the Twenty-Ninth Annual ACM-SIAM Symposium on Discrete Algorithms*, ser. SODA '18. USA: Society for Industrial and Applied Mathematics, 2018, p. 1029–1046.
- [61] G. H. Golub and C. F. Van Loan, *Matrix Computations*, 3rd ed. The Johns Hopkins University Press, 1996.

Table V: Expressions of each code and their AF [23]

Type of Code	Phase Expression	AF
Frank Sequence	$\phi_{n,k} = 2\pi \frac{(n-1) \cdot (k-1)}{L}$ <p>for $1 \leq n \leq L, 1 \leq k \leq L,$</p>	
P_x Sequence	$\phi_{n,k} = \begin{cases} \frac{2\pi}{L} \left[\left(\frac{L+1}{2} - k \right) \left(\frac{L+1}{2} - n \right) \right], & L \text{ even} \\ \frac{2\pi}{L} \left[\left(\frac{L}{2} - k \right) \left(\frac{L+1}{2} - n \right) \right], & L \text{ odd} \end{cases}$ <p>for $1 \leq n \leq L, 1 \leq k \leq L,$</p>	
P_1 Code	$\phi_{n,k} = \frac{2\pi}{L} \left[\left(\frac{L+1}{2} - n \right) ((n-1)L + (k-1)) \right]$ <p>for $1 \leq n \leq L, 1 \leq k \leq L,$</p>	
P_2 Code	$\phi_m = \frac{2\pi}{M} \left[\frac{(m-1)^2}{2} \right]$ <p>for $1 \leq m \leq M,$</p>	
P_4 Code	$\phi_m = \frac{2\pi}{M} (m-1) \left[\frac{m-1-M}{2} \right]$ <p>for $1 \leq m \leq M,$</p>	
Zadoff Code	$\phi_m = \frac{2\pi}{M} (m-1) \left[r \cdot \left(\frac{M-1-m}{2} \right) - q \right]$ <p>for $1 \leq m \leq M, 0 \leq q \leq M$ where M is any integer and r is any integer relatively prime to $M,$</p>	
Golomb Sequence	$\phi_m = \frac{2\pi}{M} r'' \left[\frac{(m-1)(m)}{2} \right]$ <p>for $1 \leq m \leq M,$ where M is any integer and r'' is any integer relatively prime to $M,$</p>	